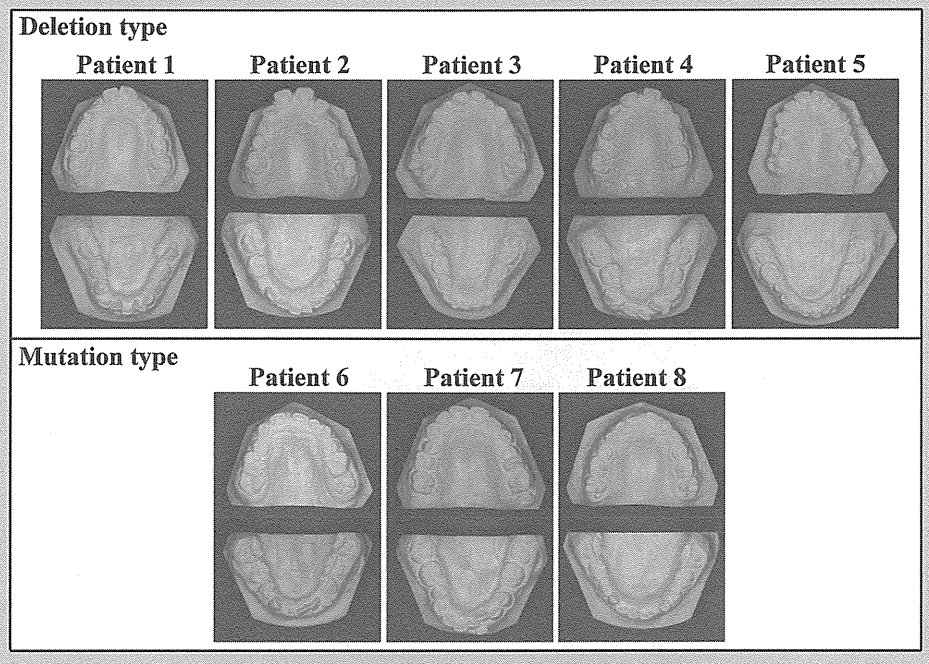

FIG. 4. Dental arch shapes of eight patients. Upper panel: maxillary dental casts, lower panel: mandibular dental casts. A narrow maxillary dental arch with labioclination of the central incisors is noted in all five deletion type patients, with the mandibula being saddle-shaped in three patients (Patients 1, 3, and 4) and U-shaped in two (Patients 2 and 5), while U-shaped upper and lower dental arches are noted in all three mutation-type patients (Patients 6, 7, and 8).

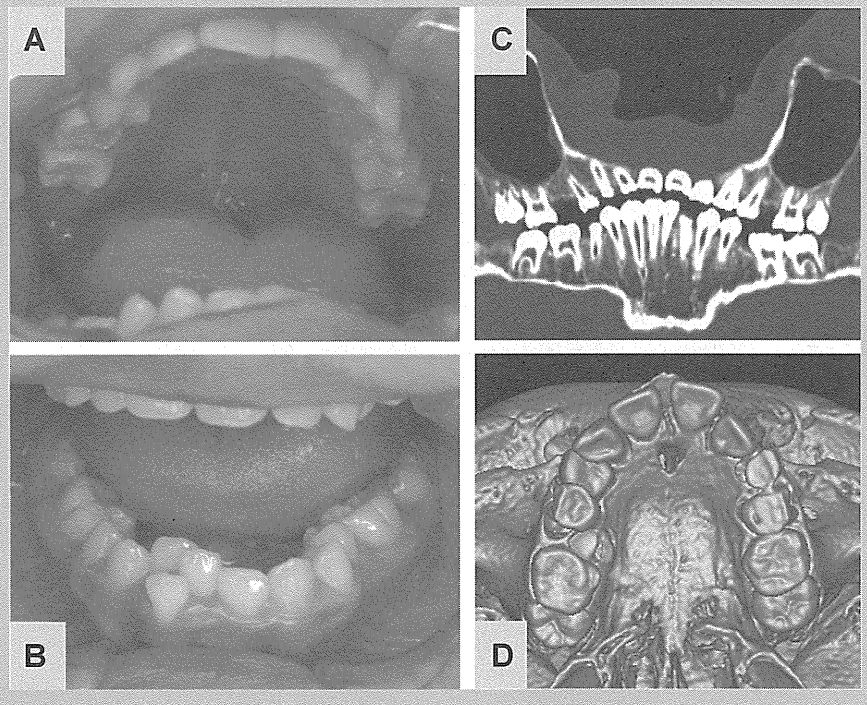

FIG. 5. Oral photographs (A,B) and MDCT-synthesized panoramic radiograph (C) of Patient 7 at age of 10 years and MDCT-synthesized upper dental arch of Patient 6 at age of 7 years (D). Note: high palate, malocclusion, small dental arch, excessive tooth wear (A,B), missing upper second premolars on both side and lower left second premolar (C), ectopic tooth eruption of first molars on both side (D).

were often difficult to perform in childhood. Thus, in this study, MDCT was used as a substitute for cephalometric radiographs and panoramic radiographs, and by which maxillofacial manifestations could be accurately evaluated [Hirai et al., 2010; Yamauchi et al., 2010].

In view of oral and dental management, we would like to provide recommendations as follows: periodic dental check up to prevent dental caries or gingivitis should be started early after one or more deciduous teeth have erupted. Around age 7 years, detailed oral and dental evaluations, including dental cast studies and MDCT, is recommended for possible hypodontia and malocclusion. If the patient has hypodontia, preceding deciduous tooth (teeth) should be maintained as long as possible with proper care. Although malocclusion like scissors bite and cross bite requires early treatment, including expansion of upper or lower jaw, to prevent craniofacial disabilities such as facial asymmetry and temporomandibular joint dysfunction, the treatment should be carefully decided based on consideration of capability of cooperation of the patients.

In conclusion, features seen more frequently and more pronounced form in deletion-type than in mutation-type were small dental arch with labioclination of the maxillary central incisors, mandibular recession, and scissors or posterior cross bite. Sotos syndrome patients should be followed closely for possible dental and oral complications especially for malocculusion in the deletion-type.

ACKNOWLEDGMENTS

The authors are grateful to Prof. Takahide Maeda for his helpful advice. We also thank to Dr. Kenji Shimizu, Dr. Yasuo Takahashi, and Hitoshi Yabe for their invaluable assistance. This study was funded in part by a Grant for the Support of Projects for Strategic Research at Private Universities by the Ministry of Education, Culture, Sports, Science and Technology (MEXT; 2008-2012), and by a grant from the Ministry of Health, Labour and Welfare, Japan.

REFERENCES

Callnan AP, Anand P, Sheehy EC. 2006. Sotos syndrome with hypodontia. Inter J Paediatri Dent 16:143–146.

Cole TRP, Hughes HE. 1994. Sotos syndrome: A study of the diagnostic criteria and natural history. J Med Genet 31:20–32.

Gomes-Silva JM, Ruviere DB, Segatto RA, de Queiroz AM, de Freitas AC. 2006. Sotos syndrome: A case report. Spec Care Dentist 26:257–262.

Grabowski R, Kundt G, Stahl F. 2007a. Interrelation between occlusal findings and orofacial myofunctional status in primary and mixed dentition: Part III: Interrelation between malocclusions and orofacial dysfunctions. J Orofac Orthop 68:462–476.

Grabowski R, Stahl F, Gaebel M, Kundt G. 2007b. Relationship between occlusal findings and orofacial myofunctional status in primary and mixed dentition. Part I: Prevalence of malocclusions. J Orofac Orthop 68:26–37.

Hirai N, Yamauchi T, Matsune K, Kobayashi R, Yabe H, Ohashi H, Maeda T. 2010. A comparison between two dimensional and three dimensional cephalometry on lateral radiographs and multi detector row computed tomography scans of human skulls. Int J Oral-Med Sci 9:101–107.

Iizuka T, Ishikawa F. 1957. Normal standards for various cephalometric analysis in Japanese adults. Nippon Kyosei Shika Gakkai Zasshi 16:4–12.

Inokuchi M, Nomura J, Mtsumura Y, Sekida M, Tagawa T. 2001. Sotos syndrome with enamel hypoplasia: A case report. J Clin Pediatr Dent 25:313–316.

Kotilainen J, Pohjola P, Pirinen S, Arte S, Nieminen P. 2009. Premolar hypodontia is a common feature in Sotos syndrome with a mutation in the NSD1 gene. Am J Med Genet Part A 149A:2409–2414.

Kurotaki N, Imaizumi K, Harada N, Masuno M, Kondoh T, Nagai T, Ohashi H, Naritomi K, Tsukahara M, Makita Y, Sugimoto T, Sonoda T, Hasegawa T, Chinen Y, Tomita HH, Kinoshita A, Yoshiura KK, Ohta T, Kishino T, Fukushima Y, Niikawa N, Matsumoto N. 2002. Haploinsufficiency of NSD1 causes Sotos syndrome. Nat Genet 30:365–366.

Nagai T, Matsumoto N, Kurotaki N, Harada N, Niikawa N, Ogata T, Imaizumi K, Kurosawa K, Kondoh T, Ohashi H, Tsukahara M, Makita Y, Sugimoto T, Sonoda T, Yokoyama T, Uetake K, Sakazume S, Fukushima Y, Naritomi K. 2003. Sotos syndrome and haploinsufficiency of NSD1: Clinical features of intragenic mutations and sub microscopic deletions. J Med Genet 40:285–289.

Nishimura K, Mori Y, Yamauchi M, Kamakura N, Homma H, Namura H, Miyamoto E, Matsumoto M, Shintani S, Ooshima T. 2008. Sotos syndrome with oligodontia: A case report. Pediatric Dent J 18:187–191.

Otsubo J. 1957. A study on the tooth material in Japanese adults of normal occlusion, its relationship to coronal and basal arches. Nippon Kyosei Shika Gakkai Zasshi 16:36–46.

Otsubo J, Ishikawa F, Kuwahara Y. 1964. A longitudinal study of dental development between 6–13 years of age: Growth changes of dentition. Nippon Kyosei Shika Gakkai Zasshi 23:182–190.

Sotos JF, Dodge PR, Muirhead Dl, Crawford JD, Talbot NB. 1964. Cerebral gigantism in childhood. A syndrome of excessively rapid growth with acromegatic features and a nonprogressive neurologic disorder. N Engl J Med 271:109–116.

Stahl F, Grabowski R, Gaebel M, Kundt G. 2007. Relationship between occlusal findings and orofacial myofunctional status in primary and mixed dentition. Part II: Prevalence of orofacial dysfunctions. J Orofac Orthop 68:74–90.

Takei K, Sueishi K, Yamaguchi H, Ohtawa Y. 2007. Dentofacial growth in patients with Sotos syndrome. Bull Tokyo Dent Coll 48:73–85.

Welbury RR, Fletcher HJ. 1988. Cerebral gigantism (Sotos syndrome) two case reports. J Paediatr Dent 4:41–44.

Yamauchi T, Hirai N, Matsune K, Kobayashi R, Yabe H, Ohashi H, Maeda T. 2010. Accuracy of tooth development stage, tooth size and dental arch width in multi detector row computed tomography scans of human skulls. Int J Oral Med Sci 9:108–114.

RESEARCH ARTICLE

AMERICAN JOURNAL OF medical genetics PART A

Delineation of Dermatan 4-*O*-Sulfotransferase 1 Deficient Ehlers–Danlos Syndrome: Observation of Two Additional Patients and Comprehensive Review of 20 Reported Patients

Kenji Shimizu,[1] Nobuhiko Okamoto,[2] Noriko Miyake,[3] Katsuaki Taira,[4] Yumiko Sato,[5] Keiko Matsuda,[2] Noriko Akimaru,[2] Hirofumi Ohashi,[1] Keiko Wakui,[6] Yoshimitsu Fukushima,[6] Naomichi Matsumoto,[3] and Tomoki Kosho[6]*

[1]Division of Medical Genetics, Saitama Children's Medical Center, Saitama, Japan

[2]Department of Medical Genetics, Osaka Medical Center and Research Institute for Maternal and Child Health, Osaka, Japan

[3]Department of Human Genetics, Yokohama City University Graduate School of Medicine, Yokohama, Japan

[4]Department of Orthopedics, Saitama Children's Medical Center, Saitama, Japan

[5]Department of Radiology, Saitama Children's Medical Center, Saitama, Japan

[6]Department of Medical Genetics, Shinshu University School of Medicine, Matsumoto, Japan

Received 20 January 2011; Accepted 21 April 2011

Loss-of-function mutations in *CHST14*, dermatan 4-*O*-sulfotransferase 1 (D4ST1) deficiency, have recently been found to cause adducted thumb-clubfoot syndrome (ATCS; OMIM-#601776) and a new type of Ehlers–Danlos syndrome (EDS) coined as EDS Kosho Type (EDSKT) [Miyake et al., 2010], as well as a subset of kyphoscoliosis type EDS without lysyl hydroxylase deficiency (EDS VIB) coined as musculocontractural EDS (MCEDS) [Malfait et al., 2010]. Lack of detailed clinical information from later childhood to adulthood in ATCS and lack of detailed clinical information from birth to early childhood in EDSKT and MCEDS have made it difficult to determine whether these disorders would be distinct clinical entities or a single clinical entity with variable expressions and with different presentations depending on the patients' ages at diagnosis. We present detailed clinical findings and courses of two additional unrelated patients, aged 2 years and 6 years, with EDSKT with a comprehensive review of 20 reported patients with D4ST1 deficiency, which supports the notion that these disorders constitute a clinically recognizable form of EDS. The disorder, preferably termed D4ST1-deficient EDS, is characterized by progressive multisystem fragility-related manifestations (joint dislocations and deformities, skin hyperextensibility, bruisability, and fragility; recurrent large subcutaneous hematomas, and other cardiac valvular, respiratory, gastrointestinal, and ophthalmological complications) resulting from impaired assembly of collagen fibrils, as well as various malformations (distinct craniofacial features, multiple congenital contractures, and congenital defects in cardiovascular, gastrointestinal, renal, ocular, and central nervous systems) resulting from inborn errors of development.

How to Cite this Article:
Shimizu K, Okamoto N, Miyake N, Taira K, Sato Y, Matsuda K, Akimaru N, Ohashi H, Wakui K, Fukushima Y, Matsumoto N, Kosho T. 2011. Delineation of dermatan 4-*O*-sulfotransferase 1 deficient Ehlers–Danlos syndrome: Observation of Two Additional Patients and Comprehensive Review of 20 Reported Patients.
Am J Med Genet Part A 155:1949–1958.

Key words: dermatan 4-*O*-sulfotransferase 1 deficiency; adducted thumb-clubfoot syndrome; Ehlers–Danlos syndrome Kosho type; musculocontractural Ehlers–Danlos syndrome; congenital contractures; progressive multisystem fragility-related manifestations; malformations

Additional supporting information may be found in the online version of this article.
Grant sponsor: Research on Intractable Diseases, Ministry of Health, Labor and Welfare, Japan; Grant number: 2141039040.
Kenji Shimizu, Nobuhiko Okamoto, and Tomoki Kosho have equally contributed to this work.
*Correspondence to:
Tomoki Kosho, MD, Department of Medical Genetics, Shinshu University School of Medicine, 3-1-1 Asahi, Matsumoto 390-8621, Japan.
E-mail: ktomoki@shinshu-u.ac.jp
Published online 8 July 2011 in Wiley Online Library (wileyonlinelibrary.com).
DOI 10.1002/ajmg.a.34115

INTRODUCTION

Dermatan 4-*O*-sulfotransferase 1 (D4ST1) is a regulatory enzyme in the glycosaminoglycan biosynthesis that transfers active sulfate to position 4 of the *N*-acetyl-D-galactosamine residues of dermatan sulfate [Evers et al., 2001; Mikami et al., 2003]. Dermatan sulfate, as well as chondroitin sulfate and heparan sulfate, constitutes glycosaminoglycan sidechains of proteoglycans; and has been implicated in cardiovascular disease, tumorigenesis, infection, wound repair, and fibrosis via dermatan sulfate-containing proteoglycans such as decorin and biglycan [Trowbridge and Gallo, 2002]. Carbohydrate sulfotransferase 14 (*CHST14*), localized on 15q12, is the gene encoding D4ST1. Recently, loss-of-function mutations in *CHST14* (D4ST1 deficiency) have been found to cause adducted thumb-clubfoot syndrome (ATCS; OMIM#601776) in 11 patients from four families [Dündar et al., 2009] and a variant of Ehlers–Danlos syndrome (EDS) in six patients from six families [Miyake et al., 2010], tentatively coined as EDS Kosho Type (EDSKT) in the London Dysmorphology Database (http://www.lmdatabases.com/index.html) and POSSUM (http://www.possum.net.au/). ATCS was originally recognized as a new type of arthrogryposis, focused on characteristic clinical pictures from birth to early childhood, including adducted thumbs and talipes equinovarus as well as facial dysmorphisms (prominent forehead, large fontanelle, hypertelorism, down-slanting palpebral fissures, low-set ears), and arachnodactyly [Dündar et al., 1997; Sonoda and Kouno, 2000; Dündar et al., 2001; Janecke et al., 2001]. In a recent study by Dündar et al. [2009], ATCS has been categorized again as a connective tissue disorder, based on additional clinical pictures from childhood to adolescence, including skin fragility and bruisability, joint laxity, and osteopenia. EDSKT comprises a pattern of distinct craniofacial features, multiple congenital contractures, progressive joint and skin laxity, and progressive multisystem fragility-related manifestations, including recurrent large subcutaneous hematomas and other cardiac, respiratory, gastrointestinal, ophthalmological complications [Yasui et al., 2003; Kosho et al., 2005, 2010].

Very recently, Malfait et al. [2010] have independently found mutations in *CHST14* in three patients from two families, who were diagnosed with kyphoscoliosis type EDS without lysyl hydroxylase deficiency (EDS VIB). They concluded that their series and ATCS, as well as EDSKT, formed a phenotypic continuum based on their clinical observations and identification of an identical mutation in both conditions, and proposed to coin the disorder as "musculocontractural EDS" (MCEDS) [Malfait et al., 2010]. However, it is still an unsolved problem whether ATCS, EDSKT, and MCEDS would be distinct clinical entities or a single clinical entity with variable inter- and intrafamilial expressions and with different presentations depending on the patients' ages at diagnosis [Miyake et al., 2010], because detailed clinical information are lacking in ATCS from later childhood to adulthood and in EDSKT and MCEDS from birth to early childhood.

Here, we present detailed clinical findings and courses of two additional unrelated patients, aged 2 years and 6 years, with EDSKT, which would contribute to delineate comprehensive phenotypic spectrum of D4ST1 deficiency.

CLINICAL REPORTS

Patient 1

The patient, a Japanese boy, was the second child of a healthy 31-year-old mother and a healthy 33-year-old nonconsanguineous father. He was born by cesarean for breech presentation at 38 weeks and 3 days of gestation. His birth weight was 3,092 g (+0.2 SD), length 46 cm (−1.3 SD), and OFC 34 cm (+0.4 SD). At age 15 days, he was referred to our hospital for the treatment of bilateral talipes equinovarus. He had a round face with a large fontanelle, hypertelorism, short palpebral fissures, blue sclerae, strabismus, a short nose with a hypoplastic columella, low-set and rotated ears, a high palate, a long philtrum, a thin upper lip vermillion, a small mouth, and microretrognathia (Fig. 1A, B). He had arachnodactyly, flexion-adduction contractures of bilateral thumbs, flexion contractures of the interphalangeal (IP) joints in the other fingers, flexion contractures of bilateral elbows and knees, and rigidity of bilateral hip joints (Fig. 1C). He also had widely spaced nipples, a redundant and translucent skin, an umbilical hernia, and bilateral cryptorchidism (Fig. 1C). Talipes equinovarus was treated with incision of bilateral Achilles' tendons at age 2 months, followed by serial plaster casts and braces. Skin fragility was observed at the procedure. It was surgically corrected at age 1 year and 11 months. Gross motor development was delayed: He raised his head at 6 months, sat without support at age 1 year, stood up assisted at age 1 year and 6 months, and walked assisted after surgical correction of talipes equinovarus. He had bruises easily on the occiput

FIG. 1. Clinical photographs of Patient 1 at age 15 days (A–C), at age 1 year and 3 months (D–G), and at age 2 years and 10 months (H–P).

and buttocks after falling, which were absorbed spontaneously. Bleeding time was 1.3 min (normal values, 1–5 min), prothrombin time-international normalized ratio (PT-INR) 1.00 (normal values, 0.81–1.38 sec), and activated partial thromboplastin time (APTT) 27.9 sec (normal values, 23–36 sec).

When seen by us at age 1 year and 3 months, his craniofacial shape became square with a broad, bossed forehead, and hypertelorism with downslanting palpebral fissures became evident (Fig. 1D, E). Skin redundancy and tapering fingers and toes were noted (Fig. 1D, F, G). Ear rotation and flexion contractures of fingers improved (Fig. 1E, F).

When last seen by us at age 2 years and 10 months, he weighed 9.86 kg (−2.4 SD), height 84.9 cm (−2.1 SD), and OFC 45.5 cm (−2.4 SD). His face was slender, and was characterized by an unclosed fontanelle, hypertelorism, short and downslanting palpebral fissures, blue sclerae, strabismus, a short nose with a hypoplastic columella, low-set ears, a high palate, a long philtrum, a thin upper lip vermillion, a small mouth, and microretrognathia (Fig. 1H). He had a Marfanoid habitus, generalized joint laxity, a flat and thin thorax, and distinctive fingers (tapering with enlargement of distal phalanges) (Fig. 1I–L), and talipes valgus and planus with extremely soft subcutaneous tissues at the heels (Fig. 1N–P). The distal IP joints in bilateral index to little fingers and the IP/metacarpophalangeal (MP) joints in bilateral thumbs could hardly be flexed or extended. The MP joints in bilateral index to little fingers could be moved with poor flexion and hyperextension (see Supplementary Video 1 online). He had hyperextensible to redundant skin with bruisability and fine palmer creases (Fig. 1J, L, M). He suffered from constipation (defecation twice a week), treated with oral magnesium oxide. Ophthalmological examinations showed mild esotropia, and amblyopia due to severe hyperopic astigmatism. A cardiac ultrasonography showed no defects or valve abnormalities but mild dilation of the ascending aorta at the sinus of Valsalva. A brain CT showed no ventricular enlargement (Fig. 3O, P). G-banded chromosomes were normal. The Kinder Infant Developmental Scale [Cheng et al., 2010] showed mild developmental delay with the overall developmental quotient as 65 (physical/motor, 35; manipulation, 58; receptive language, 77; expressive language, 103; conceptual thinking, 77; social relationships with children, 68; social relationships with adults, 116; home training, 68; feeding, 42). He had orchiopexy and a surgical correction of an umbilical hernia at age 2 years and 7 months.

Patient 2

The patient, a Japanese boy, was the first child of a healthy 25-year-old mother and a healthy 28-year-old nonconsanguineous father. He was born by normal vaginal delivery at 38 weeks of gestation. His birth weight was 2940 g (+0.3 SD), length 49.1 cm (+0.3 SD), and OFC 32 cm (−0.5 SD). He was admitted for the treatment of bilateral adducted thumbs and talipes equinovarus. His craniofacial features included a large fontanelle, a high forehead, hypertelorism, short and downslanting palpebral fissures, blue sclerae, strabismus, a short nose with a hypoplastic columella, low-set and rotated ears, a high palate, a long philtrum, a thin upper lip vermillion, a small mouth, and microretrognathia (Fig. 2A). He had arachnodactyly, flexion-adduction contractures of bilateral thumbs, flexion contractures of the IP joints in the other fingers, rigidity of bilateral hip joints, and mild pectus excavatum (Fig. 2A, B). He also had widely spaced nipples, a redundant skin, and bilateral cryptorchidism (Fig. 2A). He suckled poorly and hated to be hugged tightly, suggesting hyperalgesia to pressure. Talipes equinovarus was treated with serial plaster casts. Gross motor development was delayed: He raised his head at 7 months, sat without support at age 1 year and 2 months, crawled at age 1 year and 6 months, pulled himself up by holding to something at age 1 year and 6 months, and walked unassisted at age 2 years and 6 months. His fontanelle was closed at age 3 years.

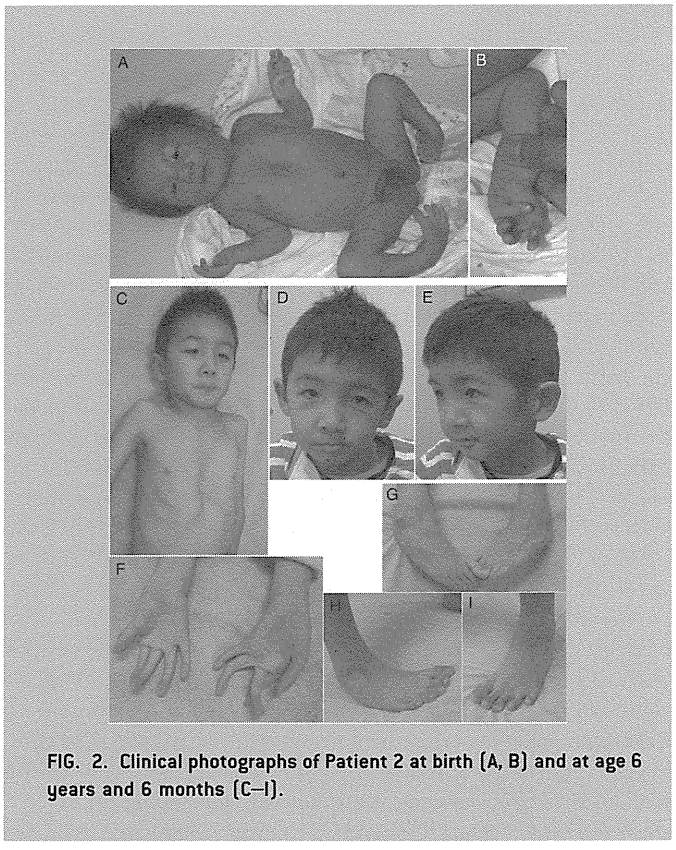

FIG. 2. Clinical photographs of Patient 2 at birth (A, B) and at age 6 years and 6 months (C–I).

At age 3 years, he developed a large subcutaneous hematoma over the skull after falling. Hematomas on the lower legs frequently occurred. He had recurrent dislocations of bilateral shoulders.

When last seen by us at age 6 years and 6 months, he weighed 16.4 kg (−1.4 SD), height 112 cm (−1.0 SD), and OFC 51.5 cm (−0.2 SD). He could jump unassisted. His craniofacial features included hypertelorism, short and downslanting palpebral fissures, blue sclerae, strabismus, a short nose with a hypoplastic columella, low-set ears, a high palate, a long philtrum, a thin upper lip vermillion, a small mouth, and microretrognathia (Fig. 2D, E). He had a Marfanoid habitus, generalized joint laxity, and pectus excavatum (Fig. 2C). His fingers were cylindrical and slender (Fig. 2F). He showed talipes equinovarus when lying down (Fig. 2G) and talipes planus when standing (Fig. 2H, I). The subcutaneous tissues at the heels were extremely soft. The distal IP joints in bilateral index to little fingers and the IP joints in bilateral thumbs

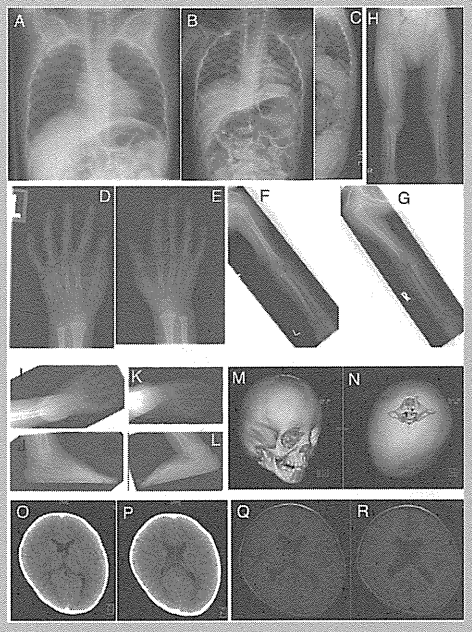

FIG. 3. Radiographs of Patient 1 at age 1 year and 10 months (A) and 2 years and 6 months (B–L). Cranial and brain CT of Patient 1 at age 2 years and 6 months (M–P). Brain MRI of Patient 2 at age 1 year and 10 months (Q, R).

could hardly be flexed or extended. The proximal IP joints in bilateral index to little fingers and the MP joints in all fingers could be flexed and extended, but could not be moved separately and smoothly. His skin was hyperextensible and bruisable. Fine palmar creases were also noted (Fig. 2F). He occasionally had constipation and abdominal pain. A cardiac ultrasonography showed trivial mitral valve prolapse, patent ductus arteriosus, and dextrocardia. A brain MRI showed bilateral ventricular enlargement (Fig. 3Q, R). G-banded chromosomes were normal. His intelligence was normal.

SKELETAL INVESTIGATIONS

Radiographs of Patient 1 were reviewed. At age 2 years and 6 months, he had mild scoliosis (Fig. 3B), which was not noted at age 1 year and 10 months (Fig. 3A). Physiological lumbar lordosis was not present (Fig. 3C). The left hip joint was dislocated (Fig. 3H). Long bones of the legs and arms showed over modeling, with narrowing diaphysis and widening metaphysis (Fig. 3F–H). Bilateral tibiae and fibulae were medially curved (Fig. 3H). Short bones of the hands (Fig. 3D, E) and feet (Fig. 3I–L) also showed over modeling, as well as osteoporotic changes in the feet (Fig. 3I–L).

MUTATION ANALYSIS

Genomic DNA was extracted from peripheral blood leukocytes of the patients and their parents, and was amplified with PCR using four primer sets for *CHST14* (sequences available on request). Through direct sequencing of the PCR products, compound heterozygous mutations were detected in both patients: c.842 C > T causing p. Pro281Leu (p.P281L) and c.878 A > G causing p.Tyr293Cys (p.Y293C) in Patient 1; c.626 T > C causing p.Phe209Ser (p.F209S) and c.842 C > T causing p.Pro281Leu (p.Y293C) in Patient 2 (data not shown). The parents had one of the two heterozygous mutations observed in their children.

DISCUSSION

We have presented detailed clinical characteristics and courses of two new unrelated pediatric patients with compound heterozygous *CHST14* mutations. The features showed striking resemblance to those of patients with EDSKT in their infancy to early childhood [Kosho et al., 2005, 2010]. *CHST14* mutations (P281L/Y293C) in Patient 1 were identical to those found in two patients with EDSKT [Miyake et al., 2010]. F209S found in Patient 2, which was not listed on a database of common gene variations in the Japanese population (JSNP) [Haga et al., 2002], was the mutation that has never found in previous patients with ATCS, EDSKT, or MCEDS.

To date, 22 patients (12 males, 10 females) from 14 families, including present patients, have been reported to have homozygous or compound heterozygous mutations in *CHST14* (Tables I and II) [Dündar et al., 1997; Sonoda and Kouno, 2000; Dündar et al., 2001; Janecke et al., 2001; Yasui et al., 2003; Kosho et al., 2005; Dündar et al., 2009; Kosho et al., 2010; Malfait et al., 2010; Miyake et al., 2010]. Eight families were of Japanese origin, three of Turkish origin, one of Austrian origin, and one of Indian origin. The median patients' age at their initial publication was 4 years and 1 month (range, 0 day–32 years): 7 months (range, 0 day–6 years) in ATCS, 12.5 years in EDSKT (range, 2 years–32 years), and 21 years (range, 12 years–22 years) in MCEDS.

CHST14 mutations included V49X in two families (ATCS, MCEDS), K69X in one (EDSKT), R135G in one (ATCS), L137Q in one (ATCS), F209S in one (EDSKT), R213P in one (ATCS), P281L in eight (EDSKT), C289S in one (EDSKT), Y293C in four (one ATCS, three EDSKT), and E334GfsX107 in one (MCEDS). Sulfotransferase activity of COS-7 cells transfected with *CHST14* containing K69X, P281L, C289S, or Y293C mutation was decreased at almost the same level, suggesting that loss-of-function mutations in *CHST14*, that is to say D4ST1 deficiency, would cause these disorders [Miyake et al., 2010].

Characteristic craniofacial features at birth to early infancy (large fontanelle, hypertelorism, short and downslanting palpebral fissures, blue sclerae, short nose with hypoplastic columella, low-set and rotated ears, high palate, long philtrum, thin upper lip vermilion, small mouth, and micro-retrognathia) were noted in most patients with ATCS, EDSKT, and MCEDS. Slender and asymmetrical facial shapes with protruding jaws from school age, commonly observed in patients with EDSKT, were also described in ATCS2 at age 15 years, ATCS3 at age 6 years, ATCS7 at age 8 years [Dündar et al., 2009], and in MCEDS1 at age 21 years [Malfait et al., 2010]. A pair of ATCS siblings had palatal defects: ATCS4 with cleft lip and palate, which was surgically repaired, and ATCS5 with cleft soft palate [Sonoda and Kouno, 2000].

Congenital multiple contractures, most specifically adduction–flexion contractures of thumbs and talipes equinovarus,

TABLE I. Clinical Characteristics of Reported Patients With D4ST1 Deficiency (Continued)

Family	Patient	Origin	*CHST14* Mutations	Age at initial publication (d, days; m, months; y, years)	Sex	Craniofacial												Skeletal							Cutaneous						Cardiovascular			Gastrointestinal		
						Large fontanelle (early childhood)	Hypertelorism	Down-slanting palpebral fissures	Blue sclerae	Short nose with hypoplastic columella	Ear deformities	Palatal abnormalities	Long philtrum and thin upper lip	Small mouth/micro-retrognathia in infancy	Short neck	Slender face/protruding jaw from school age	Facial asymmetricity from school age	Malfanoid habitus/slender build	Congenital multiple contractions	Recurrent/chronic joint dislocations	Pectus deformities	Spinal deformities	Peculiar fingers (tapering - slender and cylindrical)	Progressive talipes deformities	Hyperextensibility/ redundancy	Bruisability	Fragility/atrophic scars	Fine/Acrogeria-like palmar creases	Hyperalgesia to pressure	Recurrent subcutaneous infections/fistula	Congenital heart defects	Valve abnormalities	Large subcutaneous hematomas	(Hemo) pneumathorax	Constipation	Others
ATCS																																			
1	1	Turkish	V49X homo	3.5y	F	+	+	+	+		P, PR	H	+		+				+				+							–					
	2			1.5y	M	+	+	+	+	+	P, PR		+		+	+a		+a	+	+a	Exa	KSa	+	Planus, valgus#					+a						
	3			6y	F		+	+		+	P		+			+	+	+	+		F–T	S	+	Varus					+						
2	4	Japanese	Y293C homo	4y	M	+	+	+		+	LS	CL/CP	+						+	+	Ca		+	Planus, valgus											
	5			7m	M	+	+	+		+	LS	CSP	+						+	+			+							ASD					
3	6	Austrian	R213P homo	0d†	M	+	+	+			PR, LS				+				+			S	+							ASD, CoA					Common mesentery
	7			12m	M	+	+	+	+		D, PR				+	+a		+a	+		F–Ta		+	Planus, valgus#					+a						Absence of gastrocolic omentum, spontaneous volvulus of small intestine
4	8	Turkish	R135G / L137Q	1–4m†	F														+																
	9			1–4m†	M														+																
	10			1–4m†	M														+																
	11			3m	M	+	+	+	+		D, LS	H	+		+				+				+							–					
MCEDS																																			
1	1	Turkish	V49X homo	22y	F	+		+		+	PR, LS	H	+			+	+	+	+		F–T	KS	+	Planus, valgus	+	+	+	+		+	–	–			Hiatal hernia, gastroesphageal reflux, abdominal pain
	2			21y	F	+		+	+			H	+						+	+	F–T	S	+	Small, broad	+	+	+	+							
2	3	Indian	E334GfsX107 homo	12y	F				+		LS		–					+	+	+		KS	+	Planus, valgus	+	+	+	+		+					Duodenum obstruction due to malrotation
EDSKT																																			
1	1	Japanese	P281L / Y293C	11y	F	+	+	+	+	+	LS	H	+	+		+	+	+	+	+	Ex	KS	+	Planus, valgus	+	+	+	+	+	+	ASD	TR, TVP, MVP	+	–	+	Gastric ulcer§
2	2	Japanese	P281L homo	14y	F	+	+	+	+	+	LS	H	+	+		+	+	+	+	+	F–T	S	+	Cavus, valgus	+	+	+	+	+	+	–		+	+§	+	Diverticular perforation§
3	3	Japanese	P281L homo	32y	M	+	+	+	+	+	LS	H	+	+		+	+	+	+	+	F–T	KS	+	Planus, valgus	+	+	+	+	+	+		AR, ARD, MR	+	+	+	Diverticular perforation
4	4	Japanese	K69X / P281L	32y	M		+		+			H				+	+	+	+		Ex	KS	+	Planus, valgus	+	+	–	+	–	–			+	+	–	
5	5	Japanese	P281L / C289S	20y	F	+	+	+	+	+	LS	H	+	+		+	+	+	+	+	Ex	S	+	Planus, valgus	+	+	+	+	+	+		AR, MR, IE	+	–	+	
6	6	Japanese	P281L / Y293C	4y	F	+	+	+	+	+	LS	H	+						+		Ex	S	+	Planus	+	+	+	+	+	+			+	–	+	
Present report (EDSKT)																																			
7	7	Japanese	P281L / Y293C	2y	M	+	+	+	+	+	PR, LS	H	+	+				+	+		F–T	S	+	Planus, valgus	+	+	+	+	–	+	–	ARD	–	–	+	
8	8	Japanese	F209S / P281L	6y	M	+	+	+	+	+	PR, LS	H	+	+				+	+	+	Ex		+	Planus	+	+	–	+	+	–	PDA	MVP	+	–	+	Abdominal pain

ATCS, adducted thumb-clubfoot syndrome; EDSKT, Ehlers–Danlos Syndrome, Kosho Type; MCEDS, Musculocontractural Ehlers–Danlos Syndrome
+, present; Blank, information not available; †, died; F, female; M, male; P, prominent; PR, posteriorly rotated; LS, low set; D, dysplastic; H, high; CL, cleft lip; CP, cleft palate; CSP, cleft soft palate;
Ex, excavatum; F–T, flat and thin; Ca, carinatum; KS, kyphoscoliosis; S, scoliosis; ASD, atrial septal defect; CoA, coarctation of aorta; PDA, patent ductus arteriosus;
TR, tricuspid valve regurgitation; TVP, tricuspid valve prolapse; MVP, mitral valve prolapse; AR, aortic valve regurgitation; ARD, aortic root dilation; MR, mitral valve regurgitation; IE, infectious endocarditis
ATCS Patient 1 died at age 6 years [Dündar et al., 2009].
a, Information from reassessment by Dündar et al. [2009], describing ATCS P2 at age 15 years and ATCS P7 at age 8 years
b, Information from reassessment by Kosho et al. [2010], describing EDSKT1 at age 16 years and EDSKT2 at age 32 years.

TABLE II. Clinical Characteristics of Reported Patients With D4ST1 Deficiency

		Urogenital			Ophthalmological				Hearing impairment	Ventricular abnormalities (brain)	Development			Growth (prenatal)				Growth (postnatal)				References
Family	Patient	Nephro (Cysto) lithiasis	Cryptorchidism	Others	Breast development	Strabismus	Refractive errors	Glaucoma/elevated intraocular pressure	Others			Gross motor delay	Age of unassisted walk (y, years; m, months)	Mental delay	Gestational weeks	Birth length (centile or SD)	Birth weight (centile or SD)	Birth OFC (centile or SD)	Age (y, years; m, months)	Height (centile or SD)	Weight (centile or SD)	OFC (centile or SD)	
ATCS																							
1	1					+				Enl		+	No	+	Term				3.5y	25-50th	50th	50th	Dündar et al., 1997
	2					+		+		Asym		+		+c	Term				1.5y	50th	10th	10–25th	Dündar et al., 1997
																			15ya	25–50th	<3rd		Dündar et al., 2009
	3					+													6y	10–25th	<3rd		Dündar et al., 2009
2	4		+	Hydronephrosis										–	39wk	–0.6	–0.9	–0.8	4y2m	–3.9	–1.8	–0.9	Sonoda and Kouno, 2000
	5		+	Hydronephrosis, inguinal hernia								–		–	38wk	–1.6	–1.3	–0.5	7m	–2.1	–1.4	–1.1	Sonoda and Kouno, 2000
3	6		+	Horseshoe kidney						Enl					32wk	25th	10th	25th					Janecke et al., 2001
	7		+			+				Asym		–		–	38wk	50th	25th	50th	8ya	10-25th	<3rd		Janecke et al., 2001 Dündar et al., 2009
4	8																						Dündar et al., 2001
	9																						Dündar et al., 2001
	10																						Dündar et al., 2001
	11	+	+	Inguinal hernia						Enl, Asym									3m	<3rd	3–10th	10th	Dündar et al., 2001
MCEDS																							
1	1	+			–		My	+	Retinal detachment, pthysis bulbi	+		+	4y		42wk	±0	–0.67		22y	–2.0		±0	Malfait et al., 2010
	2	+		Hydronephrosis, renal ptosis, ureteral stenosis	–		My	+	Retinal detachment	+		+	2y		42wk				14y	+0.68		>2.0	
2	3						My		Microcornea			+			Term		–0.88						Malfait et al., 2010
EDSKT																							
1	1			Bladder dilation, recurrent UTI, involuntary contractionb	–b	+	Hy	–	Microcornea	+	Enl	+	2y	+d	42wk	–0.1	–1.3	–1.0	7y	+0.8	–1.0	±0	Kosho et al., 2005
																			11y	+0.2	–2	+0.2	Kosho et al., 2010
																			16y	+0.3	–0.4	+0.2	
2	2	+		Atonic bladder, recurrent UTI	–b	+	My, As	+b		+		+	No	–	Term		–2.0		15y	–3.2			Kosho et al., 2005 Kosho et al., 2010
3	3		+	Hypogonadism		+	My, As	–	Microphthalmia	+		+		–	40wk	+1.3	+0.5	+0.8	30y	+1.2	–1.7		Kosho et al., 2010
4	4					–	–	–	Retinal detachment	–				–					23y	–0.4	–2.4		Yasui et al., 2003 Kosho et al., 2010
5	5	+		Delayed menarche, irregular menstruation	–	+	My, As	+		–		+	2y2m	–	39wk	–1.1	–0.4	+1.0	19y	–0.1	–0.8		Kosho et al., 2010
6	6					+	My, As	+		+		+	1y5m	–	41wk	–1.2	–0.5	–0.6	4y	–1.2	–1.3	–0.9	Kosho et al., 2010
Present report																							
7	7		+			+	Hy, As, Am	–				+	No	+	38wk3d	–1.3	+0.2	+0.4	2y	–2.2	–2.4	–1.2	Patient 1
8	8		+			+				–	Enl	+	2y6m	–	38wk	+0.3	+0.3	–0.5	6y	–0.7	–1.4	+0.1	Patient 2

ATCS, adducted thumb-clubfoot syndrome; EDSKT, Ehlers-Danlos Syndrome, Kosho Type; MCEDS, Musculocontractural Ehlers-Danlos Syndome
+, present; Blank, information not available; UTI, urinary tract infection; Hy, hyperopia; My, myopia; As, astigmatism; Am, amblyopia; Enl, enlargement; Asym, asymmetry; No, not ambulant
a, Information from reassessment by Dündar et al. [2009], describing ATCS P2 at age 15 years and ATCS P7 at age 8 years.
b, Information from reassessment by Kosho et al. [2010], describing EDSKT1 at age 16 years and EDSKT at age 32 years.
c, IQ was 91 at Porteus test and 86 at Goodenough test at age 7 years and 2 months [Janecke et al., 2001];
d, mild learning dissability

were cardinal features in patients with ATCS, EDSKT, and MCEDS. Peculiar fingers described as "tapering," "slender," and "cylindrical" were also common features. Aberrant finger movement was described in EDSKT1 [Kosho et al., 2010], EDSKT7, and EDSKT8. EDSKT1, EDSKT2, EDSKT3, and EDSKT5 were found to have tendon abnormalities such as anomalous insertions of flexor muscles, which might result in contractures [Kosho et al., 2005, 2010]. In childhood, spinal deformities (scoliosis, kyphoscoliosis) and talipes deformities (planus, valgus) occurred and progressed. Malfanoid habitus, recurrent joint dislocations, and pectus deformities (flat and thin, excavatum, carinatum) were also evident. Talipes equinovarus in seven EDSKT patients and MCEDS3 was surgically repaired [Kosho et al., 2005, 2010; Malfait et al., 2010]. EDSKT3 received tendon transplantations for defects of tendons to bilateral thumbs, and EDSKT4 received surgical fixation of bilateral ankle joints as well as surgery for carpal tunnel syndrome [Kosho et al., 2010]. MCEDS1 underwent surgery for rapidly worsened kyphoscoliosis at age 14 years [Malfait et al., 2010].

Bone mineral density (BMD) was decreased in ATCS2 at age 15 years (Z score −1.6), ATCS3 at age 6 years (Z score −4.6) [Dündar et al., 2009], EDSKT2 at age 29 years (Z score −2.4 for the lumbar spine 1–4, −2.3 for the 33% radius), and EDSKT3 at age 31 years (Z score −3.7 for the lumbar spine 1–4, −3.6 for the femoral neck) [unpublished data], whereas BMD was normal in ATCS7 at age 8 years [Dündar et al., 2009] and EDSKT1 at age 15 years (Z score +1.6 for the lumbar spine 1–4, −0.9 for the femoral neck) [unpublished data]. Urine N-telopeptide of collagen type I (NTX), an osteoclast marker, was increased at 92.8 nmol BCE/mmol Cr in EDSKT1 at age 16 years, 70.3 nmol BCE/mmol Cr in EDSKT2 at age 28 years, and 238.4 nmol BCE/mmol Cr in EDSKT3 at age 31 years [unpublished data] (normal values for premenopausal females, 9.3–54.3; males, 13.0–66.2), whereas serum bone specific alkaline phosphatase (BAP), an osteoblast marker, was normal at 12.5 U/L in EDSKT1 at age 16 years, 25.6 U/L in EDSKT2 at age 28 years, and 15.1 U/L in EDSKT3 at age 31 years (normal values, 9.6–35.4) [unpublished data]. These results in biochemical markers of bone turnover suggested an increase in osteoclast activity with normal osteoblast activity, which could cause oeteopenia or osteoporosis.

Radiologically, diaphysial narrowing of phalanges and metacarpals was noted in EDSKT1 at age 11 and 16 years, EDSKT2 at age 10 and 28 years, EDSKT3 at age 31 years, EDSKT5 at age 19 years [Kosho et al., 2005, 2010], and EDSKT7 at age 2 years and 6 months. Talipes valgus and planus or cavum, with diaphysial narrowing of phalanges and metatarsals, were noted in ATCS7 at age 8 years [Dündar et al., 2009], EDSKT1 at age 11 and 16 years, EDSKT2 at age 14 and 28 years, EDSKT6 at age 4 years [Kosho et al., 2005, 2010], and EDSKT7 at age 2 years and 6 months. Tall vertebral bodies were noted in EDSKT1 at age 11 and 16 years, EDSKT2 at age 14 and 28 years, EDSKT3 at age 31 years, EDSKT4 at age 31 years, EDSKT5 at age 19 years [Kosho et al., 2005, 2010], and MCEDS2 at age 21 years [Malfait et al., 2010], whereas they were not noted in EDSKT6 at age 2 years [Kosho et al., 2010] and EDSKT7 at age 2 years and 6 months.

Cutaneous features were common in most patients with EDSKT and MCEDS, including hyperextensibility to redundancy, bruisability, fragility leading to atrophic scars, acrogeria-like fine palmar creases or wrinkles, hyperalgesia to pressure, and recurrent subcutaneous infections with fistula formation, which lead to skin defects including decubitus necessitating plastic surgery in EDSKT2 [Kosho et al., 2005, 2010]. Excessive palmar creases were observed in ATCS2, ATCS3, and ATCS7, and delayed wound healing and ecchymoses were also recorded ATCS patients [Dündar et al., 2009]. Palmar creases increased and became deeper according to the ages, as compared among photographs of EDSKT1 at age 11 and 16 years, EDSKT2 at age 5 years and 32 years, EDSKT3 at age 32 years, EDSKT5 at age 19years, and EDSKT6 at age 4 years [Kosho et al., 2005, 2010].

Seven patients with EDSKT suffered from large subcutaneous hematomas, which sometimes progressed acutely and massively to be treated intensively (admission, blood transfusion, surgical drainage). These lesions were supposed to be caused by rupture of subcutaneous arteries or veins. Hematoma formation was mentioned in a follow-up observation of ATCS patients [Dündar et al., 2009]. Bleeding time was prolonged in ATCS7 (9 min) [Dündar et al., 2009] and EDSKT4 (11 min) [Yasui et al., 2003; Kosho et al., 2010], whereas it was normal in EDSKT1 (3 min) [Kosho et al., 2005], EDSKT3 (1 min) [unpublished data], and EDSKT7 (1.3 min). EDSKT1 had, to prevent large subcutaneous hematomas, intranasal administration of 1-desamino-8-D-arginine vasopressin (DDAVP) after injuries [Kosho et al., 2005, 2010]. A large hematoma over the buttocks in EDSKT4 was treated with intranasal DDAVP and intramuscular conjugated estrogen [Yasui et al., 2003; Kosho et al., 2010].

Two ATCS and two EDSKT patients had congenital heart defects (atrial septal defect was the most common, observed in three), and five EDSKT patients had cardiac valve abnormalities. EDSKT5 suffered from infectious endocarditis probably resulting from aortic valve or mitral valve regurgitation, and underwent surgery. Three adult patients with EDSKT developed pneumothorax or hemopneumothorax, treated with chest tube drainage; and two of them suffered from diverticular perforation, treated surgically. Various gastrointestinal abnormalities were observed: Constipation in seven EDSKT patients and abdominal pain in one EDSKT and one MCEDS patients, as well as common mesentery in ATCS6, absent gastrocolic omentum and spontaneous volvulus of small intestine in ATCS7, gastric ulcer necessitating partial gastrectomy in EDSKT1, and duodenum obstruction due to malrotation treated surgically in MCEDS3 [Janecke et al., 2001; Dündar et al., 2009; Kosho et al., 2010; Malfait et al., 2010].

Urological complications included nephrolithiasis or cystolithiasis in one ATCS, two EDSKT, and two MCEDS patients; hydronephrosis in two ATCS and one MCEDS patients, dilated or atonic bladder with recurrent urinary tract infection in two EDSKT patients, and horseshoe kidney in one ATCS patient. Hydronephrosis in MCEDS2 was caused by renal ptosis and ureteral stenosis, for which a ureteral stent was placed with a laparoscopic procedure, complicated by severe hemorrhage due to excessive tissue fragility [Malfait et al., 2010].

Cryptorchidism was observed in five ATCS and three EDSKT male patients. EDSKT3, who received orchiopexy, showed hypogonadism in adulthood. In female patients older than adolescence, poor breast development was noted in three EDSKT (EDSKT1 and

EDSKT2 showed normal menstruation cycles; EDSKT5 showed delayed menarche and irregular menstruation cycles) and two MCEDS patients. No female patients have been reported to be pregnant.

Various ophthalmological complications were observed: Strabismus in four ATCS and seven EDSKT patients, refractive errors in six EDSKT and three MCEDS patients, glaucoma or elevated intraocular pressure in one ATCS, three EDSKT, and two MCEDS patients; microcornea or microphthalmia in two EDSKT and one MCEDS patients, and retinal detachment in one EDSKT and two MCEDS. Retinal detachment in EDSKT4 [Kosho et al., 2010] and glaucoma in MCEDS1 [Malfait et al., 2010] required surgery. Hearing impairment was noted in four EDSKT patients (predominantly for high-pitched sound in EDSKT1, EDSKT2, and EDSKT6) and two MCEDS.

Gross motor developmental delay was observed in two ATCS, seven EDSKT, and three MCEDS patients; and ages of unassisted walk in patients who accomplished it ranged from 1 year and 5 months to 4 years (median, 2 years and 1 month). EDSKT2, at age 32 years, could not walk unassisted because of severe foot deformities and muscle weakness of the legs [Kosho et al., 2010]. An underlying myopathic process was suggested in ATCS2 because of reduced amplitude muscle action potentials with normal distal latency time and nerve conduction velocity, whereas muscle biopsy did not reveal any histological abnormality [Dündar et al., 1997]. Mild mental delay was suggested in two ATCS and two EDSKT patients. ATCS2 was reported to have global psychomotor delay at the initial publication [Dündar et al., 1997], whereas his IQ was around 90 at age 7 years and 2 months [Janecke et al., 2001]. Five ATCS and two EDSKT patients showed ventricular enlargement and/or asymmetry on brain ultrasonography, CT or MRI. ATCS7 also showed absence of the left septum pellucidum [Janecke et al., 2001]. EDSKT6 had tethering of a spinal cord, and underwent duraplasty [Kosho et al., 2010].

Growth assessment was performed using data described with SD scores, excluding data described with centile scores. Patients with *CHST14* mutations showed mild prenatal growth retardation: The mean birth length −0.5 SD and the median −0.6 SD (n = 9; range, −1.6 SD to +1.3 SD); the mean birth weight −0.6 SD and the median −0.67 SD (n = 11; range, −2.0 SD to +0.5 SD); and the mean birth OFC −0.2 SD and the median −0.5 SD (n = 8; range, −1.0 SD to +1.0 SD). Postnatal growth was also mildly impaired with slenderness and relative macrocephaly: The mean height −0.9 SD and the median −0.6 SD (14 data from 12 patients; range, −3.9 SD to +1.2 SD); the mean weight −1.5 SD and the median −1.4 SD (11 data from 9 patients; range, −2.4 SD to −0.4 SD); the mean OFC −0.2 SD and the median ±0 SD (10 data from 8 patients; range, −1.2 SD to >2.0 SD).

Light microscopic investigations on skin specimens from EDSKT5 and EDSKT6 showed that fine collagen fibers were predominant in the reticular to papillary dermis and normally thick collagen bundles were markedly reduced [Miyake et al., 2010]. Electron microscopic investigations of the specimens showed that collagen fibrils were dispersed in the reticular dermis, compared with regularly and tightly assembled ones observed in the control, whereas each collagen fibril was smooth and round, not varying in size and shape, similar to each fibril of the control [Miyake et al., 2010]. These findings suggested that the main pathological basis of this disorder would be insufficient assembly of collagen fibrils, compatible with the evidence that dermatan sulfate of decorin proteoglycan, a key regulator of collagen fibril assembly that contains both chondroitin sulfate and dermatan sulfate in its glycosaminoglycan chains and controls the distance between collagen fibrils, was found to be completely lost and replaced by chondroitin sulfate in patients' fibroblasts [Miyake et al., 2010]. However, both light microscopic and electron microscopic findings of skin were assessed as normal in ATCS7 [Dündar et al., 2009]. In MCEDS2, most collagen bundles were small-sized, some of which were composed of variable diameter collagen fibrils separated by irregular interfibrillar spaces [Malfait et al., 2010].

This comprehensive review of the patients with loss-of-function mutations in *CHST14* (D4ST1 deficiency) supports the notion that ATCS, EDSKT, and MCEDS would be a single clinical entity with variable inter- and intra-familial expressions and with different presentations depending on the patients' ages at diagnosis or at publication. The disorder, we preferably would like to coin simply as EDS due to D4ST1 deficiency or D4ST1 deficient EDS (DD-EDS), is a clinically recognizable syndrome, characterized by progressive multisystem fragility-related manifestations including joint dislocations and deformities, skin hyperextensibility, bruisability, and fragility; recurrent large subcutaneous hematomas, and other cardiac valvular, respiratory, gastrointestinal, and ocular complications, which are considered to result from connective tissue weakness and be consequences of insufficient decorin-mediated assembly of collagen fibrils caused by D4ST1 deficiency. The disorder also shows various malformations including distinct craniofacial features, multiple congenital contractures, and congenital defects in cardiovascular, gastrointestinal, renal, ocular, and central nervous systems, which might not simply be accountable for connective tissue weakness but could be considered as inborn errors of development. In a recent review focusing on ATCS, Zhang et al. [2010] state that D4ST1 deficiency is the only recognized condition resulting from a defect specific to DS biosynthesis, and that the disorder emphasizes the roles D4ST1 play in human development and extracellular matrix maintenance.

DD-EDS could be detected at birth from characteristic craniofacial and skeletal features and molecular genetic testing gives definitive diagnosis. Initial screening for congenital cardiac, ocular, and renal abnormalities and hearing loss would be necessary. In infancy, orthopedic intervention for talipes equinovarus (serial plaster casts, surgery) as well as physical therapy for motor developmental delay would be the center of management. Laxatives and/or enema are considered in patients with constipation. Surgical fixation is considered for cryptorchidism in males. Regular follow-up for ophthalmological (strabismus, refractive errors, glaucoma), otological (otitis media with effusion, hearing loss), urological (urination, bladder enlargement), and cardiovascular (valve abnormalities, aortic root dilation) problems should be continued. After walking independently, attention should be paid to progressive foot deformities and trauma that could cause skin lacerations, joint dislocations, and massive subcutaneous hematomas. Intranasal DDAVP after injuries is considered to prevent large subcutaneous hematomas. From adolescence, assessment of spinal deformities (scoliosis, kyphoscoliosis) and secondary sex

characteristics (breast development in females and gonadal function in males) would be necessary. In adulthood, appropriate treatments should be performed on occasional emergency complications ([hemo]peumothorax, diverticular perforation). Wrist-type sphygmomanometer would be suitable for patients with hyperalgesia to pressure [unpublished observation].

Very recently, Janecke et al. [2011] have claimed that it would lead to confusion for clinicians and researchers to categorize the D4ST1 deficiency into a type of EDS and that an appropriate term should be "Dermatan sulfate-deficient adducted thumb-clubfoot syndrome." The reasons were described as follows: Clinically, "adducted thumb" and "clubfoot" would be the most distinguishable features at birth; etiologically, the molecular basis would differ substantially from EDS. In reply to the article, we have presented sufficient evidences for categorizing the disorder into a type of EDS: Clinically, the disorder would satisfy all the hallmarks of EDS (skin hyperextensibility, joint hypermobility, and tissue fragility affecting the skin, ligaments, joints, blood vessels, and internal organs), and the patients should be treated as having generalized connective tissue fragility in the lifelong management; etiologically, multisystem fragility in the disorder was found to be caused by impaired assembly of collagen fibrils caused by dermatan sulfate loss in the decorin glycosaminoglycan chain [Kosho et al., submitted].

In conclusion, ATCS, EDSKT, and MCEDS; which were found independently to be caused by D4ST1 deficiency, would be a single clinical entity with variable expressions and with different presentations depending on the patients' ages. The syndrome is characterized by a unique set of clinical features including progressive multisystem fragility-related manifestations (joint dislocations and deformities, skin hyperextensibility, bruisability, and fragility; recurrent large subcutaneous hematomas, and other cardiac valvular, respiratory, gastrointestinal, and ocular complications) resulting from impaired assembly of collagen fibrils, as well as various malformations (craniofacial features, multiple congenital contractures, and congenital defects in cardiovascular, gastrointestinal, renal, ocular, and central nervous systems) resulting from inborn errors of development.

ACKNOWLEDGMENTS

The authors express their gratitude to the patients and their families for participating in this study. They are also thankful to Dr. Inaba (Department of Pediatrics, Shinshu University School of Medicine) for his comments on a neurological assessment and Miss Kunimi for her technical assistance. This work was mainly supported by Research on Intractable Diseases from Japanese Ministry of Health, Welfare, and Labor (#2141039040) (N.O., N. Miyake, Y.F., N. Matsumoto, T.K.).

REFERENCES

Cheng S, Maeda T, Yamagata Z, Tomiwa K, Yamakawa N. Japan Children's Study Group. 2010. Comparison of factors contributing to developmental attainment of children between 9 and 18 months. J Epidemiol 20:S452–S458.

Dündar M, Demiryilmaz F, Demiryilmaz I, Kumandas S, Erkilic K, Kendirch M, Tuncel M, Ozyazgan I, Tolmie JL. 1997. An autosomal recessive adducted thumb-club foot syndrome observed in Turkish cousins. Clin Genet 51:61–64.

Dündar M, Kurtoglu S, Elmas B, Demiryilmaz F, Candemir Z, Ozkul Y, Durak AC. 2001. A case with adducted thumb and club foot syndrome. Clin Dysmorphol 10:291–293.

Dündar M, Müller T, Zhang Q, Pan J, Steinmann B, Vodopiutz J, Gruber R, Sonoda T, Krabichler B, Utermann G, Baenziger JU, Zhang L, Janecke AR. 2009. Loss of dermatan-4-sulfotransferase 1 function results in adducted thumb-clubfoot syndrome. Am J Hum Genet 85:873–882.

Evers MR, Xia G, Kang HG, Schachner M, Baeziger JU. 2001. Molecular cloning and characterization of a dermatan-specific *N*-acetylgalactosamine 4-O-sulfotransferase. J Biol Chem 276:36344–36353.

Haga H, Yamada R, Ohnishi Y, Nakamura Y, Tanaka T. 2002. Gene-based SNP discovery as part of the Japanese Millennium Genome Project: Identification of 190,562 genetic variations in the human genome. J Hum Genet 47:605–610.

Janecke AR, Unsinn K, Kreczy A, Baldissera I, Gassner I, Neu N, Utermann G, Müller T. 2001. Adducted thumb-club foot syndrome in sibs of a consanguineous Austrian family. J Med Genet 38:265–269.

Janecke AR, Baenziger JU, Müller T, Dündar M. 2011. Letter to the Editors. Loss of dermatan-4-sulfotransferase 1 (D4ST1/*CHST14*) function represents the first dermatan sulfate biosynthesis defect, "Dermatan sulfate-deficient adducted thumb-clubfoot syndrome." Hum Mutat 32:484–485.

Kosho T, Takahashi J, Ohashi H, Nishimura G, Kato H, Fukushima Y. 2005. Ehlers-Danlos syndrome type VIB with characteristic facies, decreased curvatures of the spinal column, and joint contractures in two unrelated girls. Am J Med Genet Part A 138A:282–287.

Kosho T, Miyake N, Hatamochi A, Takahashi J, Kato H, Miyahara T, Igawa Y, Yasui H, Ishida T, Ono K, Kosuda T, Inoue A, Kohyama M, Hattori T, Ohashi H, Nishimura G, Kawamura R, Wakui K, Fukushima Y, Matsumoto N. 2010. A new Ehlers-Danlos syndrome with craniofacial characteristics, multiple congenital contractures, progressive joint and skin laxity, and multisystem fragility-related manifestations. Am J Med Genet Part A 152A:1333–1346.

Kosho T, Miyake N, Mizumoto S, Hatamochi A, Fukushima Y, Sugahara K, Matsumoto N. 2011. A response to: Loss of dermatan-4-sulfotransferase 1 (D4ST1/*CHST14*) function represents the first dermatan sulfate biosynthesis defect, "Dermatan sulfate-deficient adducted thumb-clubfoot syndrome". Which name is appropriate, "adducted thumb-clubfoot syndrome" or "Ehlers-Danlos syndrome"? (submitted).

Malfait F, Syx D, Vlummens P, Symoens S, Nampoothiri S, Hermanns-Lê Van Lear L, De Paepe A. 2010. Musculocontractural Ehlers-Danlos syndrome (former EDS type VIB) and adducted thumb clubfoot syndrome (ATCS) represent a single clinical entity caused by mutations in the dermatan-4-sulfotransferase 1 encoding *CHST14* gene. Hum Mutat 31:1233–1239.

Mikami T, Mizumoto S, Kago N, Kitagawa H, Sugahara K. 2003. Specificities of three distinct human chondroitin/dermatan N-acetylgalactosamine 4-O-sulfotransferases demonstrated using partially desulfated dermatan sulfate as an acceptor: Implication of differential roles in dermatan sulfate biosynthesis. J Biol Chem 278:36115–36127.

Miyake N, Kosho T, Mizumoto S, Furuichi T, Hatamochi A, Nagashima Y, Arai E, Takahashi K, Kawamura R, Wakui K, Takahashi J, Kato H, Yasui H, Ishida T, Ohashi H, Nishimura G, Shiina M, Saitsu H, Tsurusaki Y, Doi H, Fukushima Y, Ikegawa S, Yamada S, Sugahara K, Matsumoto N. 2010. Loss-of-function mutations of *CHST14* in a new type of Ehles-Danlos syndrome. Hum Mutat 31:966–974.

Sonoda T, Kouno K. 2000. Two brothers with distal arthrogryposis, peculiar facial appearance, cleft palate, short stature, hydronephrosis,

retentio testis, and normal intelligence: A new type of distal arthrogryposis? Am J Med Genet 91:280–285.

Trowbridge JM, Gallo RL. 2002. Dermatan sulfate: New functions from an old glycosaminoglycan. Glycobiol 12:117R–125R.

Yasui H, Adachi Y, Minami T, Ishida T, Kato Y, Imai K. 2003. Combination therapy of DDAVP and conjugated estrogens for a recurrent large subcutaneous hematoma in Ehlers-Danlos syndrome. Am J Hematol 72:71–72.

Zhang L, Müller T, Baenziger JU, Janecke AR. 2010. Congenital disorders of glycosylation with emphasis on loss of dermatan-4-sulfotransferase? Prog Mol Biol Transl Sci 93:289–307.

Hum Genet (2012) 131:121–130
DOI 10.1007/s00439-011-1051-4

ORIGINAL INVESTIGATION

Spread of X-chromosome inactivation into chromosome 15 is associated with Prader–Willi syndrome phenotype in a boy with a t(X;15)(p21.1;q11.2) translocation

Satoru Sakazume · Hirofumi Ohashi · Yuki Sasaki · Naoki Harada · Katsumi Nakanishi · Hidenori Sato · Mitsuru Emi · Kazushi Endoh · Ryoichi Sohma · Yasuhiro Kido · Toshiro Nagai · Takeo Kubota

Received: 25 February 2011 / Accepted: 19 June 2011 / Published online: 7 July 2011

Abstract X-chromosome inactivation (XCI) is an essential mechanism in females that compensates for the genome imbalance between females and males. It is known that XCI can spread into an autosome of patients with X;autosome translocations. The subject was a 5-year-old boy with Prader–Willi syndrome (PWS)-like features including hypotonia, hypo-genitalism, hypo-pigmentation, and developmental delay. G-banding, fluorescent in situ hybridization, BrdU-incorporated replication, human androgen receptor gene locus assay, SNP microarrays, ChIP-on-chip assay, bisulfite sequencing, and real-time RT-PCR were performed. Cytogenetic analyses revealed that the karyotype was 46,XY,der(X)t(X;15)(p21.1;q11.2),−15. In the derivative chromosome, the X and half of the chromosome 15 segments showed late replication. The X segment was maternal, and the chromosome 15 region was paternal, indicating its post-zygotic origin. The two chromosome 15s had a biparental origin. The DNA methylation level was relatively high in the region proximal from the breakpoint, and the level decreased toward the middle of the chromosome 15 region; however, scattered areas of hypermethylation were found in the distal region. The promoter regions of the imprinted *SNRPN* and the non-imprinted *OCA2* genes were completely and half methylated, respectively. However, no methylation was found in the adjacent imprinted gene *UBE3A*, which contained a lower density of LINE1 repeats. Our findings suggest that XCI spread into the paternal chromosome 15 led to the aberrant hypermethylation of *SNRPN* and *OCA2* and their decreased expression, which contributes to the PWS-like features and hypo-pigmentation of the patient. To our knowledge, this is the first chromosome-wide methylation study in which the DNA methylation level is demonstrated in an autosome subject to XCI.

Electronic supplementary material The online version of this article (doi:10.1007/s00439-011-1051-4) contains supplementary material, which is available to authorized users.

S. Sakazume (✉) · R. Sohma · Y. Kido · T. Nagai
Division of Pediatrics, Dokkyo University Koshigaya Hospital, 2-1-50 Minami Koshigaya, Koshigaya, Saitama 343-8555, Japan
e-mail: saka343@dokkyomed.ac.jp

H. Ohashi
Division of Genetics, Saitama Children's Medical Center, Hasuda, Japan

Y. Sasaki · N. Harada
Department of Molecular Genetic Research and Analysis, Advanced Medical Science Research Center, Mitsubishi Chemical Medience Corporation, Tokyo, Japan

K. Nakanishi · H. Sato · M. Emi
DNA Chip Research Inc, Yokohama, Japan

H. Sato · M. Emi
Department of Neurology, Hematology, Metabolism, Endocrinology and Diabetology, Yamagata University School of Medicine, Yamagata, Japan

K. Endoh · T. Kubota
Department of Epigenetic Medicine, Faculty of Medicine, Interdisciplinary Graduate School of Medicine and Engineering, University of Yamanashi, Chuo, Japan

Introduction

X-chromosome inactivation (XCI) is a genetic mechanism in females in which one of the two X chromosomes are stochastically inactivated in the early stages of embryonic development. In each cell, the inactivated X-chromosome is randomly chosen; therefore, paternal and maternal X chromosomes have a 50% probability of being inactivated, and females are functional mosaic of two cell populations (Lyon 1961, 1962).

XCI is an essential mechanism for normal development that contributes to gene-dosage compensation process in females (Takagi and Abe 1990). Failure of XCI in females leads to embryonic lethality or abortion on the basis of observations in the embryos of cloned animals (Xue et al. 2002; Yang et al. 2007) or severe phenotypes at birth in humans (Schmidt and Du Sart 1992; Kubota et al. 2002). X-inactivation is mediated by the X inactive-specific transcript gene (*XIST*), a cis-acting RNA molecule (Brown et al. 1991). Studies using ectopic mouse *Xist* integrated into an autosome have demonstrated that *Xist* RNA coats the transgenic autosomes, leading to the reduced expression of genes over 50 cM, and suggest that long-range cis effects occur on the autosome (Herzing et al. 1997; Lee and Jaenisch 1997; Lee et al. 1996). In this report, we describe a boy with t(X;15)(p21.1;q11.2), and analyze the breakpoints, status of the *XIST* gene, extent of XCI spread on an autosome using the DNA methylation status at the CpG islands of genes related to the patient's clinical features. To date, only three studies have measured the spread of X inactivation by gene expression analysis using a somatic cell hybrid that carries the translocated chromosome (Giorda et al. 2008; White et al. 1998) or allele-specific quantitative RT-PCR using heterozygous polymorphism (Sharp et al. 2002). In this report, we investigate how XCI spreads in an autosome using a microarray-based method. To our knowledge, this is the first report that demonstrates the level and extent of XCI in an autosome at a chromosome-wide level in terms of DNA methylation.

Methods

Chromosome and fluorescent in situ hybridization (FISH) analyses

High-resolution G-banded chromosomes were prepared from peripheral blood lymphocytes according to standard procedures. FISH using bacterial artificial chromosome (BAC) DNA as a probe was performed on metaphase chromosomes of the patient with der (X). Chromosome slides were pre-incubated in 2× SSC at 37°C for 30 min, denatured in 70% formamide with 2× SSC at 72°C for 2 min, and then dehydrated at −20°C in ethanol. Cloned DNA was labeled with SpectrumGreen TM-11-dUTP or SpectrumOrange TM-11-dUTP (Vysis, Downers Grove, IL, USA) by nick translation and denatured at 76°C for 10 min. The probe-hybridization mixture (10 mL) was applied to the chromosomes, and they were incubated at 37°C for 16 h. Slides were washed three times in 4× SSC, 0.1% Tween-20 at 45°C and mounted in an anti-fade solution (Vector, Burlingame, CA, USA) containing DAPI.

We used 32 BAC clones to confirm the break point of the X chromosome and to confirm the presence of the *XIST* gene in the der (X). We also used 12 BAC clones to confirm the breakpoint of chromosome 15. The BAC clones, their locations, and the containing gene are shown in Supplemental Table 1. All of the clones were selected using the UCSC genome browser database (http://genome.ucsc.edu).

Quantitative RT-PCR analysis

Total RNA was isolated using the RNeasy Mini Kit (Qiagen, Hilden, Germany) according to the manufacturer's instruction. Reverse transcription and real-time RT-PCR were carried out using SYBR ExScript RT-PCR Kit (Takara, Kyoto, Japan). Quantitative real-time RT-PCR analysis was performed in triplicate with an Applied Biosystems (Foster City, CA, USA) Prism 7700 Sequence detection system according to the manufacturer's instructions. The mRNA expression levels, normalized against those of the corresponding *GAPDH* mRNA levels, were relatively quantified. The primer pairs used for the *GAPDH* and *OCA2* genes were GAPDH (HA031578, Takara) and OCA2 (HA032005, Takara), respectively, and the primer sequences for the *XIST* gene were: XIST-113202F, 5′-GCAGTTTGCCCTACTAGCTCCT-3′ and XIST-11456R, 5′-TCCTCAGGTCTCACATGCTCA-3′.

X-chromosome inactivation analyses

Replication R-banding study was performed on chromosomes stained with DAPI as described elsewhere (Uehara et al. 2001).

The human androgen receptor gene locus (HUMARA) assay using methylation-specific PCR was performed as described previously (Kubota et al. 1999). Briefly, the assay uses a bisulfite-treatment followed by PCR, and we obtained the inactive X pattern based on the methylated allele at the HUMARA locus and the active X pattern based on the unmethylated allele at the same locus. Both patterns were used to calculate the XCI ratio (Kubota et al. 1999).

Methylated DNA immunoprecipitation (MeDIP) assay using a human CpG island microarray

The methylation status of the CpG islands (CGIs) was analyzed using the methylated DNA immunoprecipitation method with a human CGI oligonucleotide microarray system according to the manufacturer's protocol (Agilent Technologies, Santa Clara, CA, USA). Briefly, sonicated genomic DNA was prepared and used for immunoprecipitation with a 5-methylcytidine monoclonal antibody (BI-MECY-1000) (Eurogentec, Seraing, Belgium). We

labeled 250 ng of methylation-enriched DNA samples and reference (input, non-enriched control) DNA samples, which were not amplified, with Cy3 and Cy5, respectively, using an Agilent Genomic DNA Labeling Kit PLUS (Agilent Technologies). Labeled DNA was hybridized to the custom array containing 5,859 high-density probes specific for the CpG promoters on chromosome 15, which was designed using the eArray Agilent web-based database (hg18, NCBI 36.3) on a 44K platform CpG promoter microarray. The array was scanned with an Agilent G2565BA microarray scanner (Agilent Technologies). All experiments were performed in duplicate. We compared methylation between the patient and two normal controls, according to the previously described methodology (Sharp et al. 2010).

Bisulfite DNA sequencing

Genomic DNA was extracted from peripheral lymphocytes, and bisulfite treatment of genomic DNA was performed using the EpiTect Bisulfite Kit (Qiagen) according to the manufacturer's instructions. Primers for the bisulfite genomic sequencing PCR were designed using the online program MethPrimer (http://www.urogene.org/methprimer/index1.html). The amplified PCR products were sequenced using the following primers:

SNRPN-F, 5′-AAAAACTTTAAAACCCAAATTCC-3′;
SNRPN-R, 5′-GTGGGGTTTTAGGGGTTTAGTA-3′;
UBE3A-F, 5′-TTCTAACACCAACCCCTTC-3′;
UBE3A-R, 5′-AGTTTTTY (C and T) GGTGTGGATA GGTA-3′;
OCA2-F, 5′-TGTGTTTGTGTTGTAGGAGGGGT-3′;
OCA2-R, 5′-CCCACAAAACTACCCACATAACC-3′;
UBR1-F, 5′-AATATTTTTTGGGGTTTGTAGGT GA-3′;
UBR1-R, 5′-CAAAACCAACACTAAACAAAACCT C-3′;
TRIP15-F, 5′-GAAAGGGTAAAGTTAGGGTTTAT AT-3′;
and TRIP15-R, 5′-CCTACTTCTCCAACAAAAAAA AA-3′.

Single nucleotide polymorphism (SNP) analysis using a microarray

SNPs on chromosome 15 were analyzed using the Human 317K-Duo Bead chip array, and SNP genotypes were determined using the GenomeStudio software (Illumina, San Diego, CA, USA). More than 317,000 tagSNPs markers on this chip were selected using the database of the International HapMap Project Phase I and Phase II (NCBI build 36.3/hg18).

Genomic search for transposable elements

The UCSC data (NCBI 36.3/hg18) were searched for LINE1 (L1), Mammalian-wide Interspersed Repeat (MIR), and Alu transposable elements using the RepeatMasker Program (Ver. 3.2.7). We focused on the *SNRPN*, *UBE3A*, and *OCA2* genes, and plotted the elements using the R program (Ver. 2.10).

Results

Proband

The male proband was a 5-year-old boy and the only child of healthy and non-consanguineous parents. The pregnancy was not eventful and he was born at the 41st week of gestation and weighed 2,933 g. Body length and head circumference were at the 50th percentile (49 and 35.5 cm, respectively). Hypotonia was prominent and nasogastric tube was required for feeding during the neonatal period. PWS-like dysmorphic features were noted, including small mouth, micrognathia, rocker-bottom feet, hypopigmented hair, cryptorchidism, and hypogenitalism. Abdominal ultrasound revealed a horseshoe kidney, while head MRI demonstrated hypo-plastic corpus callosum and occipital arachnid cyst. He had severe motor developmental delay and spastic quadriplegia: at the age of 20 months he could not control his head and could not roll over. A wheelchair was required to move and continuous drainage of saliva was necessary due to difficulties with swallowing.

Cytogenetic analysis

High-resolution G-banding showed an abnormal karyotype: 46,XY,der(X)t(X;15),−15 in all 50 cells analyzed (Fig. 1a). Karyotypes of both parents were normal (data not shown). To confirm the break point of the derivative X chromosome in the patient, FISH analyses were performed, in which a series of BAC probes to the X chromosome were hybridized on metaphase spreads of the patient's lymphocytes. As a result, the signals from the RP11-172M3 probe (SpectrumOrange), mapping to Xp21.2, and from RP11-134B11 (SpectrumGreen), mapping to Xp21.1, were detected on the normal X chromosome, whereas only signal from RP11-134B11 (SpectrumGreen), mapping to Xp21.1, was detected on the derivative X chromosome, indicating that the break point of the derivative X was located between these probes (Xp21.2-p21.1 region) (Fig. 1b). Likewise, the signals from the RP11-79C23 probe (SpectrumOrange), mapping to 15q11.1-11.2, and from RP11-357P4 (SpectrumGreen), mapping to 15q11.2, were detected on the normal chromosome 15, whereas only signal from RP11-357P41 (SpectrumGreen), mapping to 15q11.2, was detected on the

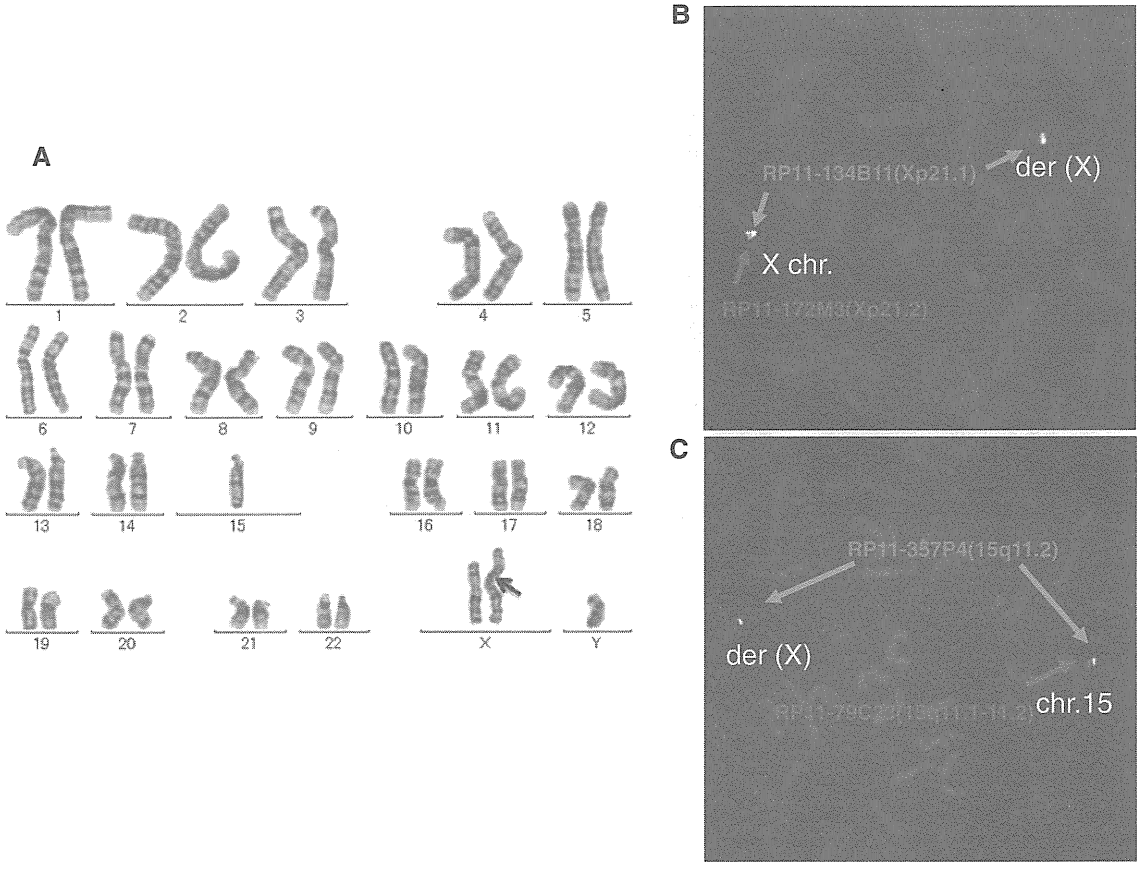

Fig. 1 Cytogenetic analyses of the patient. **a** GTG-banded full karyotype of the patient. No mosaicism was found in the 50 cells examined. An *arrow* indicates the breakpoint of the derivative X chromosome. **b** FISH analysis using the RP11-172M3 probe (SpectrumOrange) at Xp21.2 (a signal shown in *red*) and the RP11-134B11 probe (SpectrumGreen) at Xp21.1 (two signals shown in *green*). The presence of a *green* signal, but not a *red* signal, in the derivative X chromosome (der (X)) indicate that the breakpoint is located between the two probes (Xp21.2-p21.1). **c** FISH analysis using the RP11-79C23 probe (SpectrumOrange) at 15q11.1-q11.2 (a signal shown in *red*) and the RP11-357P4 probe (SpectrumGreen) at 15q11.2 (two signals shown in *green*). The presence of a *green* signal, but not a *red* signal, in the derivative X chromosome (der (X)) indicate that the breakpoint is located between the two probes (15q11.1-q11.2)

derivative X chromosome, indicating that the break point of the derivative X was located between these probes (15q11.2) (Fig. 1c). Taken together, the patient's karyotype was interpreted as 46,XY,der(X)t(X;15)(p21.1;q11.2),−15.

SNP analysis of chromosome 15

To determine the parental origin of the chromosomes 15 in the patient, we examined the 9303 SNPs on chromosome 15 and found that 444 SNPs demonstrated the biparental inheritance of chromosome 15 in the patient (Table S2). The remaining SNPs were uninformative and none showed uniparental origin. Since the SNRPN gene promoter region was extremely methylated, in which the normally unmethylated paternal allele was methylated presumably due to XCI, the chromosome 15 region in the derivative X was determined to be of paternal origin. Therefore, together with the results of the HUMARA assay, in which the normal X and derivative X chromosomes were maternal, SNP analysis suggests that the derivative X consisted of the maternal X chromosome and the paternal chromosome 15.

X-chromosome inactivation analysis

To examine the XCI status in the derivative X chromosome, we first performed FISH analysis with a BAC probe containing the *XIST* gene to confirm its presence. As a result, the signal from the BAC probe RP11-13M9 (SpectrumGreen) was retained in the normal and derivative X chromosomes, as was the signal from the X-chromosome control probe RP11-402H20 (SpectrumOrange) at the Xq subtelomeric region (Fig. 2a). Replication R banding analysis demonstrated that the derivative X chromosome was inactivated, and this inactivation covered the X chromosome and the proximal 15q region; however, the inactivation did not spread distal to 15q in all the 100 cells

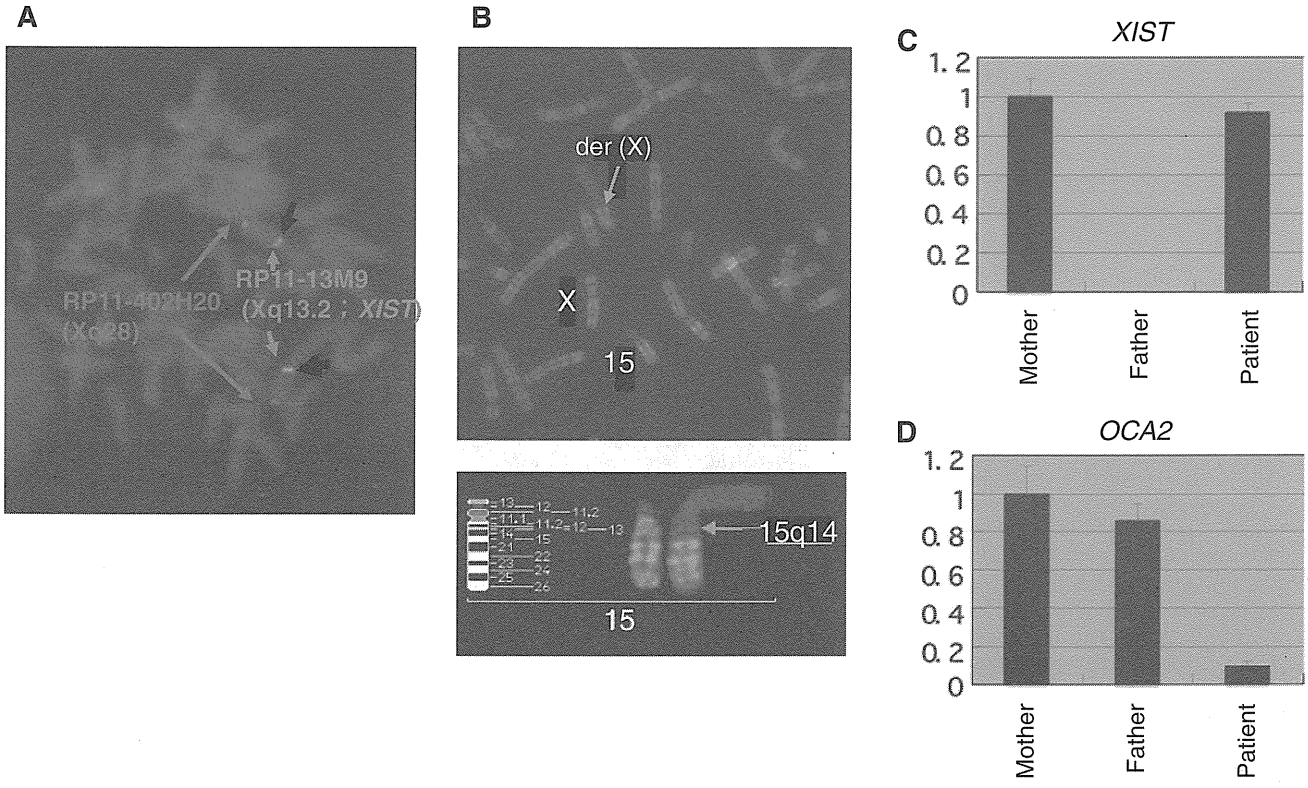

Fig. 2 Cytogenetic analysis for X-chromosome inactivation. **a** FISH analysis using the RP11-13M9 probe (SpectrumGreen), covering the *XIST* gene (two signals shown in *green*) and the RP11-402H20 probe (SpectrumOrange), located at the Xq-subtelomeric region (two signals shown in *red*), indicating that the derivative and normal X chromosomes have an *XIST* gene. **b** Replication R-banding study in the patient. A late replication/no banded segment was observed in the derivative X chromosome beyond the 15q14 region, which was assessed by the R-banding pattern of the normal chromosome 15 (see *lower enlarged panel*). **c** Real-time RT-PCR assay for *XIST* gene expression in the patient and parents. **d** Real-time RT-PCR assay for *OCA2* gene expression in the patient and parents. The *axis* represents the relative expression level for the mother (**c**, **d**)

examined (Fig. 2b, upper and lower panels with enlargement). We also confirmed *XIST* gene expression in the patient using real-time RT-PCR at almost the same level as in the mother, a normal female (Fig. 2c), suggesting *XIST* expression from the allele on the derivative X chromosome.

The HUMARA assay showed that the patient had a relatively non-random (skewed) XCI pattern (89:11) whereas the mother had a random XCI pattern (41:59). In addition, two copies of the HUMARA gene locus (Xq12) were inherited from the mother and no copy was inherited from the father (Fig. 3). These data indicate that the XIST gene was expressed from the derivative X, leading to the XCI effect spreading to the middle of the chromosome 15 in the derivative X beyond the break point, and also indicate that the normal and derivative X chromosomes were transmitted from the mother. The relatively skewed inactivation pattern in the patient was consistent with the result of the replication study, in which one X (presumably the derivative X) was preferentially inactivated in all cells examined.

DNA methylation analyses of CGIs on chromosome 15 of the derivative X chromosome

To further understand the spread of XCI on the chromosome 15 of the derivative X in terms of DNA methylation, we performed MeDIP analysis using CGI microarray to identify CGI hypermethylated regions in the patient in comparison with two healthy male controls (Fig. 4, upper panel). As a result, we observed constant CGI hypermethylation from the break point, beyond the *OCA2* locus (15q12), to 15q14 [40 Mb from the centromere]. In the middle of 15q, from 15q21.1 [50 Mb] to 15q22.2 [60 Mb], including *UBR1* (15q15.2) and *TRIP15* (15q21.1), CGI hypermethylation was rarely detected. However, scattered CGI hypermethylation was observed in the remaining telomeric region distal to 15q22.2 [60 Mb] in the patient (Fig. 4, upper panel).

In the proximal region, the CGIs of *SNRPN*, *ATP10A*, and *OCA2* were hypermethylated in the patient, whereas that of *UBE3A*, which was located in the middle of these

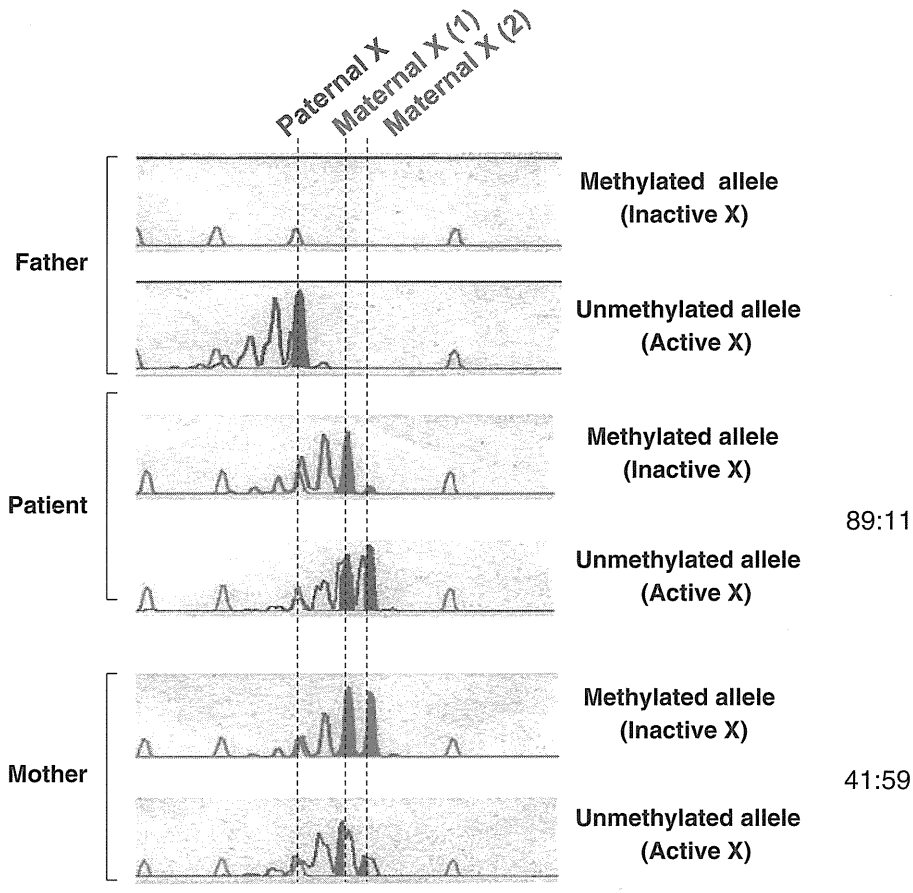

Fig. 3 Molecular analysis of X-chromosome inactivation. The HUMARA assay, based on methylation-specific PCR, demonstrates that the peak area of "Maternal X (1)" is much larger than that of "Maternal X (2)" in the methylated allele (Inactive X) lane in the patient, indicating relatively non-random (skewed) inactivation (89:11). However, the peak area of "Maternal X (1)" is affected by a shadow peak of "Maternal X (2)" in the unmethylated allele (Active X) lane, by PCR slippage error at the triplet repeat locus, because the allele difference between "Maternal X (1)" and "Maternal X (2)" is only 3 base pairs (1 triplet). Therefore, in this case, we only consider the result in the methylated allele (Inactive X) lane. In the mother, the patterns of the peak area of "Maternal X (1)" and "Maternal X (2)" are similar between the methylated (Inactive X) and unmethylated allele (Active X) lanes, indicating random inactivation (41:59). In the father, no peak is detected in the methylated allele (Inactive X) lane and only 1 peak is detected in the unmethylated allele (Active X) lane, as expected

genes, was not hypermethylated (Fig. 4, middle panel). In the middle region, the CGIs of *UBR1* and *TRIP15* were not hypermethylated in the patient (Fig. 4, middle panel).

Bisulfite sequencing analyses confirmed the results obtained from the MeDIP analysis. The CGI of *SNRPN* was extensively hypermethylated in the patient, whereas a healthy control showed ~50% methylation. Since *SNRPN* is an imprinted gene in which only the maternal allele is hypermethylated, this observation suggests that the normally unmethylated paternal allele (presumably the allele on the derivative X) was methylated in the patient (Fig. 3, lower panel). In the CGI of *OCA2*, the patient showed ~50% methylation whereas the control was not methylated, indicating that one of the two alleles (presumably the allele on the derivative X) was hypermethylated in the patient (Fig. 4, lower panel). This observation was consistent with the lower expression level of this gene in the patient (Fig. 2e). Taken together, the CGIs of the genes at 15q11.2-12 were hypermethylated presumably due to the spread of XCI in the derivative X.

However, the CGI of *UBE3A* was not shown to be hypermethylated by either the microarray assay or bisulfite sequencing analysis (Fig. 4, middle and lower panels); however, CGIs of the adjacent genes, *SNRPN* and *ATP10A*, were hypermethylated (Fig. 4, middle panel), indicating that the CGI of *UBE3A* might have some mechanism to escape the X-inactivation effect. We observed a lower density of LINE-1 and Alu elements in the upstream region of UBE3A (GenBank Accession No.: NM_000462) (Fig. 4, light blue area) compared with that in the upstream region of SNRPN (GenBank Accession No.: NM_003097) (Fig. 5, light pink area). As for MIR elements, no difference was found between these regions and both regions only contained a few MIR elements (Fig. 5).

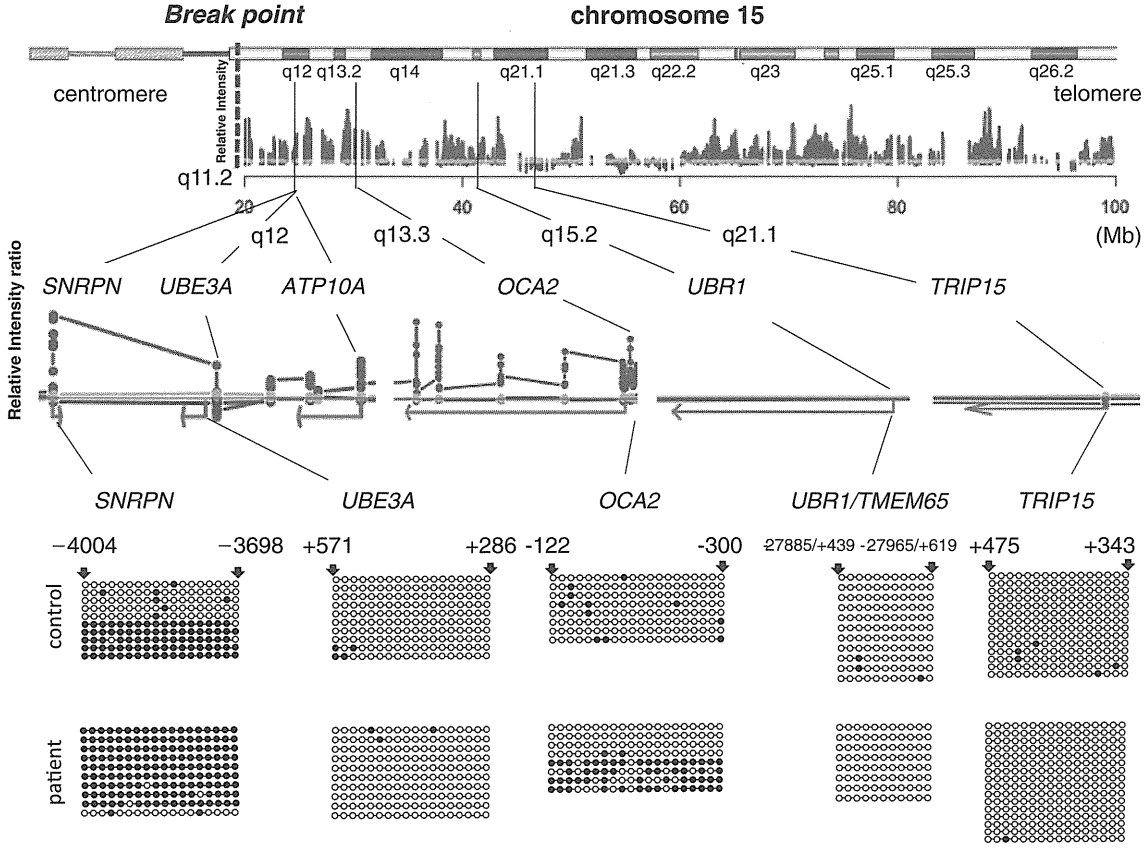

Fig. 4 DNA methylation analyses of CGIs in the chromosome 15 of the derivative X chromosome. *Upper panel*: profile of the DNA methylation difference between the chromosome 15 segment of the patient's derivative X chromosome and the chromosomes 15s of two healthy controls obtained by MeDIP analysis using CGI microarray analysis. *Middle panel*: enlarged view of the MeDIP analysis for genes on chromosome 15. *Spots* indicate the genomic positions of the oligonucleotides used for hybridization in the microarray assay, were designed within the CGIs of the genes. The *red arrows* indicate the transcriptional direction of the genes. The averages of hybridization determine the level of DNA methylation, which is shown as a *green* or *blue line*. *Lower panel*: bisulfite sequences of the CGIs on chromosome 15. *Open circle*: hypo-methylated CpG, *closed circle*: hypermethylated CpG. Genomic locations of the first and the last CpG in the sequence analyzed from the transcriptional start site are designated above the bisulfite sequence results

As expected, the CGIs of the genes in the distal region, *UBR1* and *TRIP15*, were not methylated (Fig. 4, middle and lower panels).

Distribution of transposable elements

We observed a high density of L1 elements in the upstream regions of the *SNRPN* and *OCA2* genes. However, the L1 density was low in the upstream region of the *UBE3A* gene. MIR elements were rarely detected in the upstream regions of all three genes. A high density of Alu transposable elements was observed in the upstream regions of the *SNRPN* gene, but not in the upstream regions of the *OCA2* and *UBE3A* genes.

Discussion

We molecularly characterized of the spread of XCI in an autosome of a boy with a t(X;15)(p21.1;q11.2) translocation. In this study, we found that (1) the *XIST* gene was active in the derivative X chromosome; (2) XCI and CGI hypermethylation constantly extended into the proximal region of the chromosome 15 section of the derivative X (breakpoint: ~15q14 [40 Mb from the centromere]); (3) CGI hypermethylation was not observed in the middle of 15q (15q21.1 [50 Mb]: q22.2 [60 Mb]); and (4) scattered CGI methylation was found in the distal 15q region (15q22.2 [60 Mb]: telomere). The CGI of *UBE3A* was not hypermethylated, although those of adjacent genes [e.g., the imprinted *SNRPN* gene and non-imprinted *ATP10A* (normally unmethylated)] (DuBose et al. 2010) were aberrantly hypermethylated. These results indicate that the spread of XCI from a translocated X chromosome is limited and gradually decreases (although it depends on the gene) in an autosome (Fig. 6).

As for the clinical relevance of these findings, the copy of Xq was completely inactivated in most of the cells, probably due to the selection of cells in which the derivative X

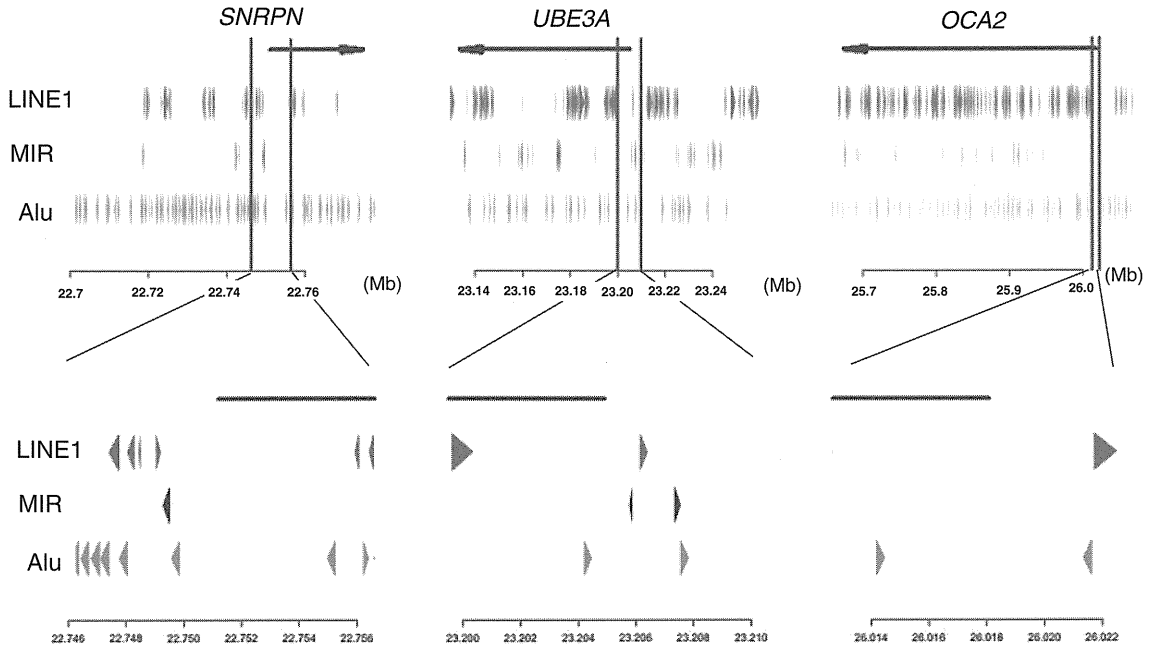

Fig. 5 Schematic illustration of the density of L1, MIR, and Alu repetitive sequences in the regions surrounding the transcription start sites of the *SNRPN*, *UBE3A*, and *OCA2* genes. A *triangle* (*red*, *black*, or *green*, respectively) indicates LINE1, MIR, or Alu sequences. The *direction* of each triangle indicates the transcriptional direction. The *SNRPN*, *UBE3A*, and *OCA2* gene regions are shown by the *arrows* at the *top*. The physical distance (Mb) from the telomere of the short arm of chromosome 15 is shown at the *bottom*

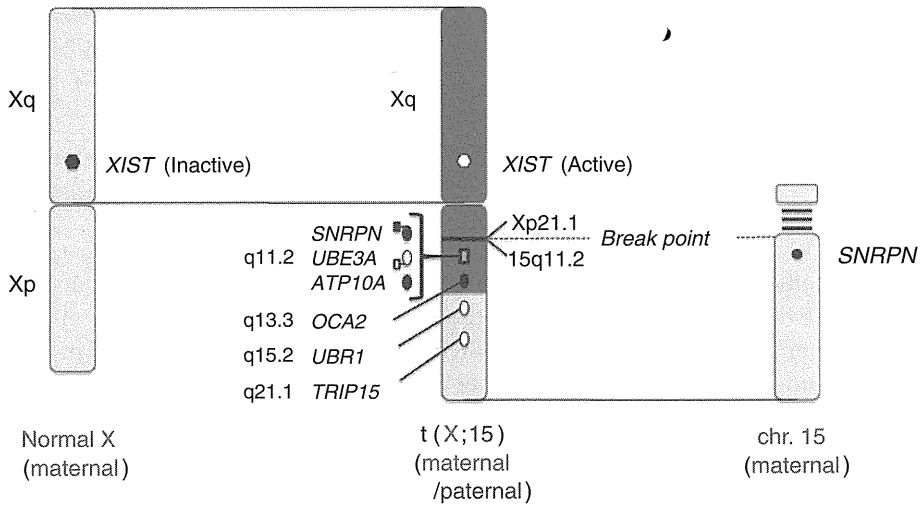

Fig. 6 Schematic representation of the molecular characterization of the patient with a t(X;15)(p21.1;q11.2) translocation. *Open circle* (*oval* and *hexagon*): hypo-methylated (active) gene, *closed circle* (*oval* and *hexagon*): hypermethylated (inactive) gene. *Open* and *closed squares* indicate low density and high density of LINE1 copies in the promoter regions of the genes, respectively

was active and the normal X was inactive during early development. Thus, some of the patient's clinical features should be due to gene inactivation caused by the spread of XCI, including *OCA2* and *SNRPN*, which may contribute to the hypo-pigmentation of the patient's skin and hair (Akahoshi et al. 2001; Brilliant et al. 1994) and the Prader–Willi syndrome-like features, respectively.

Wirth et al. reported a case with a translocation between chromosomes X and 15 [t(X;15)(q28;q12)]. In this case, the translocation was balanced (no monosomy), The XCI pattern was random (42:58), and XCI did not spread into the chromosome 15 part of the derivative X chromosome (Wirth et al. 2001). Because *SNRPN* and the adjacent *HBII-85* C/D box snoRNA (a transcript presumably related to the PWS phenotype) were disrupted by the breakpoint located in 15q12, the patient showed PWS-like features, such as obesity with an obsession for food, hypogonadism, and mental retardation at the age of 20 years, but did not have characteristic facial features, neonatal episodes of muscular hypotonia or failure to thrive. On the other hand, our patient's condition was more severe than the case of Wirth et al. and had features not described in that study, probably